

## Article

# Green Synthesis of Silver Oxide Microparticles Using Green Tea Leaves Extract for an Efficient Removal of Malachite Green from Water: Synergistic Effect of Persulfate

Iqra<sup>1</sup>, Rozina Khattak<sup>1,\*</sup>, Bushra Begum<sup>1,\*</sup>, Raina Aman Qazi<sup>1</sup>, Hajera Gul<sup>1</sup>, Muhammad Sufaid Khan<sup>2</sup>, Sanaullah Khan<sup>3,4</sup>, Naheed Bibi<sup>1</sup>, Changseok Han<sup>5,6</sup> and Najeeb Ur Rahman<sup>2</sup>

<sup>1</sup> Department of Chemistry, Shaheed Benazir Bhutto Women University, Peshawar 25000, Pakistan

<sup>2</sup> Department of Chemistry, University of Malakand, Chakdara 18800, Pakistan

<sup>3</sup> Department of Chemistry, Women University Swabi, Swabi 23430, Pakistan

<sup>4</sup> Department of Biochemistry, Women University Swabi, Swabi 23430, Pakistan

<sup>5</sup> Department of Environmental Engineering, INHA University, Incheon 22212, Republic of Korea

<sup>6</sup> Program in Environmental & Polymer Engineering, Graduate School, INHA University, Incheon 22212, Republic of Korea

\* Correspondence: rznkhattak@sbbwu.edu.pk or rznkhattak@yahoo.com (R.K.); bushrachem@sbbwu.edu.pk (B.B.)

**Abstract:** The removal of water pollutants by photocatalysis is a promising technique, mainly due to its environmentally friendly and sustainable nature. In this study, the degradation of a recalcitrant organic pollutant, malachite green (MG), was investigated in water by a microstructured silver oxide photocatalyst. The silver oxide (Ag<sub>2</sub>O) microparticles (MPs) were synthesized by a low-cost, green method, mediated by green tea leaves extract. The surface, morphological and optical properties of the synthesized Ag<sub>2</sub>O MPs were determined by scanning electron microscopy (SEM), energy dispersive X-ray (EDX) analysis, X-ray diffraction (XRD) analysis, Fourier transform infrared (FTIR) spectroscopy, and ultraviolet-visible (UV-visible) spectrophotometry. The synthesized Ag<sub>2</sub>O MPs showed good photoactivity, represented by 83% degradation of malachite green (MG) ([C]<sub>0</sub> = 0.4 mM, Ag<sub>2</sub>O loading = 0.1 g L<sup>-1</sup>) at neutral pH, in 3 h. Persulfate ions (PS) showed a strong synergistic effect on the efficiency of solar/Ag<sub>2</sub>O photocatalysis, represented by complete MG removal in 15 min, in the presence of 1.6 mM PS. The results revealed that solar/Ag<sub>2</sub>O, particularly solar/Ag<sub>2</sub>O/PS photocatalysis is a promising method for the elimination of toxic organic pollutants, such as malachite green, from the water environment.

**Keywords:** water pollution; malachite green; advanced oxidation process; Ag<sub>2</sub>O photocatalysis; persulfate synergism; water treatment



**Citation:** Iqra; Khattak, R.; Begum, B.; Qazi, R.A.; Gul, H.; Khan, M.S.; Khan, S.; Bibi, N.; Han, C.; Rahman, N.U. Green Synthesis of Silver Oxide Microparticles Using Green Tea Leaves Extract for an Efficient Removal of Malachite Green from Water: Synergistic Effect of Persulfate. *Catalysts* **2023**, *13*, 227. <https://doi.org/10.3390/catal13020227>

Academic Editor: Antonio Eduardo Palomares

Received: 27 October 2022

Revised: 12 January 2023

Accepted: 17 January 2023

Published: 18 January 2023



**Copyright:** © 2023 by the authors. Licensee MDPI, Basel, Switzerland. This article is an open access article distributed under the terms and conditions of the Creative Commons Attribution (CC BY) license (<https://creativecommons.org/licenses/by/4.0/>).

## 1. Introduction

Freshwater resources, especially groundwater, are heavily polluted by the synthetic organic dyes discharged from various industries, particularly textiles, paint, cosmetics, and paper industries [1]. A large amount of synthetic organic dyes is regularly produced, mainly for dyeing, staining, or coloring purposes, ultimately entering the environment, especially water systems [2]. Many synthetic dyes are toxic organic compounds and cause severe health problems to human beings and animals, including immunological, reproductive, and developmental abnormalities, as well as carcinogenic and mutagenic activity [1,3–5]. Thus, water pollution by synthetic dyes is a big risk to the environment.

Malachite green (MG) is an organic dye extensively used in staining cotton, fabrics, silk, and leather [2]. MG is used in the production of paints and inks [6]. MG is also used as an antimicrobial agent in aquaculture [5]. It is a toxic compound of significant environmental concern [7]. Particularly, MG causes risks to human beings, including immunology, reproductive system, and liver issues [3], developmental abnormalities, and

carcinogenesis [4]. The removal of toxic organic dyes, especially malachite green (MG), from water is a critical task, and several different methods, including adsorption [8,9], microbial [10], and advanced oxidation processes (AOPs) [11–13], have been employed. Among them, advanced oxidation processes (AOPs) were promising techniques because they have low process complexity, produce less harmful by-products, are cost-effective, and have been found to be highly efficient for the removal of toxic organic pollutants [14]. Many pollutants are difficult to remove using only physical, chemical, or biological means in many water and wastewater treatment applications. A more powerful oxidation process, known as advanced oxidation, is required for more efficient removal. AOP produces strong oxidizing agents with the potential to reduce pollutant levels from hundreds of parts per million (ppm) to a few parts per billion (ppb). These radicals attack almost all organic materials because they are non-selective. These contaminants form intermediates after being broken down by the radical once. The intermediates then react with the oxidants to form stable compounds. Some well-known oxidizing agents include hydrogen peroxide, peroxymonosulfate, and persulfate, which degrade organic pollutants relatively efficiently and rapidly when photocatalysts such as metal oxides or Fe(II) in the Fenton or photo Fenton process are used [15–18].

The advanced oxidation processes (AOPs) are represented by Fenton's and photo-Fenton's processes [19,20], ionizing radiation [21], and photocatalysis [22,23]. A common characteristic of the advanced oxidation processes (AOPs) is the generation of highly oxidizing species, mostly hydroxyl radical ( $\text{HO}^\bullet$ ) and/or sulfate radical anion ( $\text{SO}_4^{\bullet-}$ ) [24]. Both hydroxyl radical ( $\text{HO}^\bullet$ ) and sulfate radical anion ( $\text{SO}_4^{\bullet-}$ ) have high oxidation potential, i.e.,  $E^\circ(\text{SO}_4^{\bullet-}) = 2.4 \text{ V}$  and  $E^\circ(\text{HO}^\bullet) = 2.7 \text{ V}$ , and are abundantly used for the oxidation and/or degradation of the most organic pollutants [25]. Advancement and development in the field of advanced oxidation processes (AOPs), mainly for environmental and sustainable purposes, is a rising research field, and solar photocatalysis is one of the most promising options [14].

Solar photocatalytic advanced oxidation processes (AOPs) are efficient methods for the degradation of recalcitrant organic pollutants in water, such as pesticides, pharmaceuticals, and dyes [22]. Different photocatalysts, such as  $\text{TiO}_2$  [26], iron [27], silver [9], zinc [28], palladium [29], and gold [30] nanoparticles, have been used for decomposing toxic organic dyes in water. Metal oxide nanoparticles are considered useful photocatalysts in the dyes' degradation and microbial inactivation [31].

To synthesize metal oxide nanoparticles or microparticles with photocatalytic applications, green synthesis methods using plant extracts are an emerging field due to their simplicity and high productivity [31]. Unlike physicochemical methods, green synthesis produces no hazardous products or by-products [32]. As a result, green synthesis of nanoparticles using various types of plant extract has been reported [33]. One such example is the synthesis of silver oxide ( $\text{Ag}_2\text{O}$ ) nanoparticles [34,35], which is environmentally friendly, cost-effective, biodegradable, and easily accessible for large-scale application [36]. Silver oxide nanoparticles were synthesized using Genwa Leaf [37] and *Phoenix dactylifera L.* [38]. Similarly, green tea leaf extract was used to synthesize gold nanoparticles (GNP) [39]. The organic coating on the surface of green synthesized nanoparticles, which makes them more stable than chemically produced nanoparticles, is the most important factor to consider [35]. As a result, silver oxide microparticles were greenly synthesized in this study, and their photocatalytic applications were revealed, considering the economic feasibility, environmental friendliness, and simple approach.

This study describes a low-cost green synthesis of silver oxide microparticles ( $\text{Ag}_2\text{O}$  MPs) that employs green tea leaf extract as a reducing and stabilizing agent. SEM, EDX, XRD, FTIR, and UV-visible spectrophotometric techniques were used to identify the structural, morphological, and optical properties of the synthesized  $\text{Ag}_2\text{O}$  MPs. The photocatalytic efficiency of the synthesized  $\text{Ag}_2\text{O}$  MPs in solar radiation was investigated for the degradation of a model organic dye, malachite green (MG), in water. Furthermore, the synergistic effect of persulfate (PS) on the efficiency of solar/ $\text{Ag}_2\text{O}$  photocatalysis for

MG degradation was determined. The results showed that solar/ $\text{Ag}_2\text{O}$  photocatalysis, particularly the solar/ $\text{Ag}_2\text{O}/\text{PS}$  system, is a promising method for completely removing toxic organic pollutants from the water environment, such as malachite green.

## 2. Results and Discussion

### 2.1. Characterization Studies

The structure, morphology, and optical properties of the synthesized  $\text{Ag}_2\text{O}$  MPs were studied by FTIR, XRD, SEM/EDX, and UV/Vis spectrophotometric techniques, and the results are discussed in the succeeding section.

#### 2.1.1. Optical Study

The UV-visible and energy band gap spectra of  $\text{Ag}_2\text{O}$  MPs are shown in Figure 1a,b, respectively. Figure 1a shows a sharp absorbance spectrum at 304 nm, which indicates the presence of silver oxide microparticles. However, Figure 1b shows a 3.95 eV energy band gap for silver oxide microparticles, which was calculated by using Tauc equation  $\alpha h\nu = A [h\nu - E_g]^n$ ; where  $\alpha$  is the absorption coefficient,  $h\nu$  is the incident photon energy, A is the constant,  $E_g$  is the energy band gap, and n is an index with a value 2 [40].

#### 2.1.2. FTIR Study

The FTIR spectrum of the synthesized  $\text{Ag}_2\text{O}$  MPs is shown in Figure 2. The bands observed at  $1065$  and  $516\text{ cm}^{-1}$  may be assigned to O-Ag-O and Ag-O vibrations [41] existing in  $\text{Ag}_2\text{O}$  MPs, synthesized from green tea leaf extract. The other peaks obtained were probably due to the green tea leaf extract and silver nitrate used in the synthesis process.

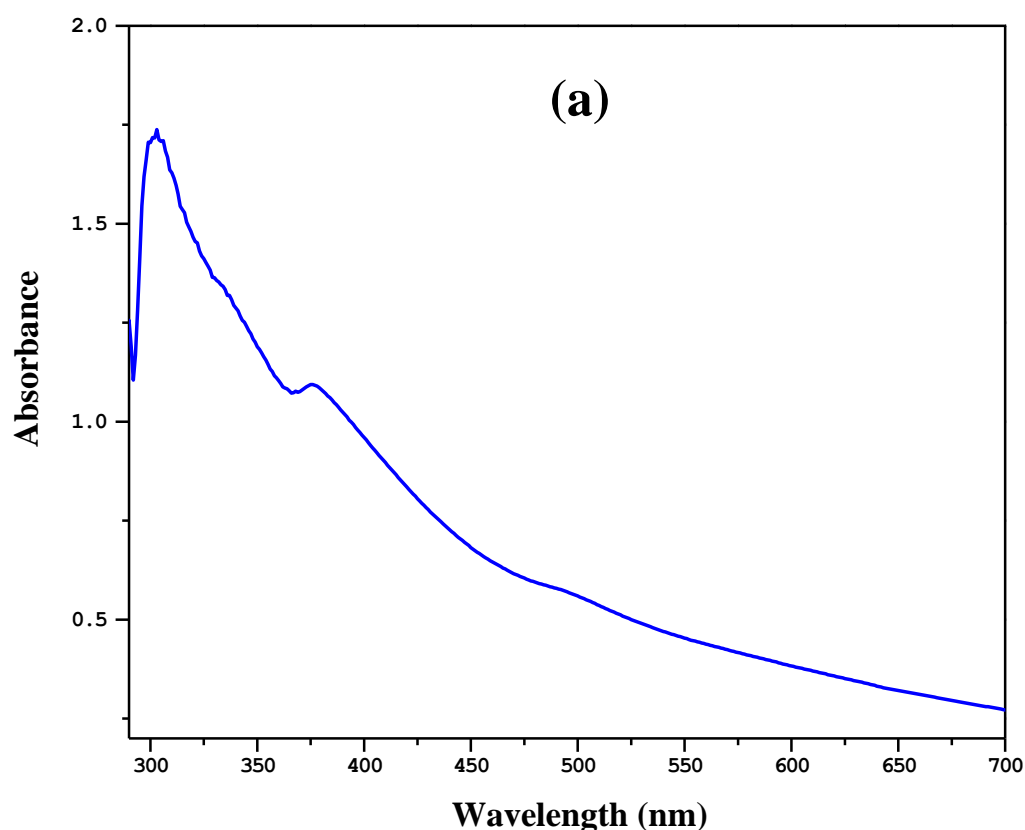


Figure 1. Cont.

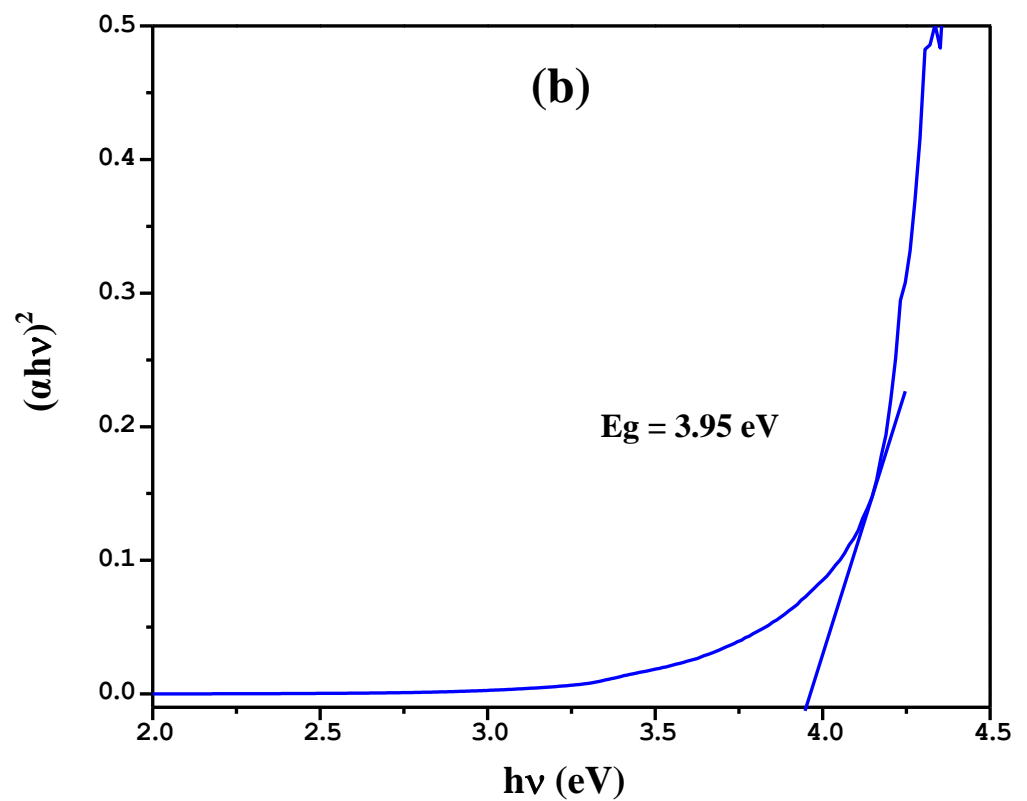


Figure 1. (a) UV-visible spectrum of  $\text{Ag}_2\text{O}$  microparticle. (b) Band gap energy of  $\text{Ag}_2\text{O}$  microparticle.

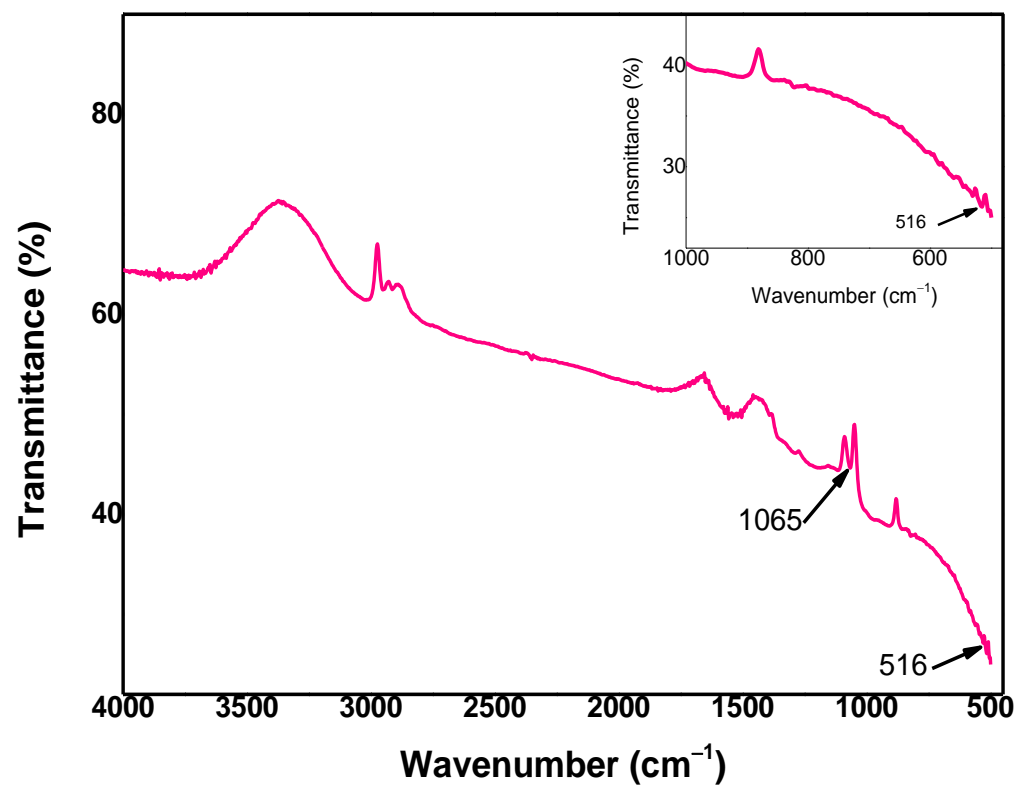


Figure 2. FTIR spectrum of silver oxide microparticles. Inset shows an enlarged view of fingerprint region of FTIR ( $1000$  to  $500 \text{ cm}^{-1}$ ).

### 2.1.3. X-Ray Diffraction Analysis

Figure 3 represents the X-ray diffraction spectrum of Ag<sub>2</sub>O MPs. The spectrum is consistent with the standard spectrum of Ag<sub>2</sub>O MPs cited in the literature. The characteristic peaks of diffraction at two theta values confirmed the Miller indices (hkl) of Ag<sub>2</sub>O MPs were 27.8° (100), 32.2° (110), 38.2° (111), 44.2° (200), 64.5° (220), and 79.5° (311) analogous with JCPDS card number 00-076-1393 [42]. The crystallite size of Ag<sub>2</sub>O MPs was 7.95 nm, as calculated by Deby-Scherrer Equation (1).

$$\tau = \kappa\lambda/\beta\cos\theta \quad (1)$$

where 'τ' is the size of the particle, 'κ' is the Scherrer's constant (κ= 0.94), 'λ' is the X-ray wavelength (1.54178Å), 'β' is full width at half maximum of the diffraction peak, and 'θ' is the Bragg angle.

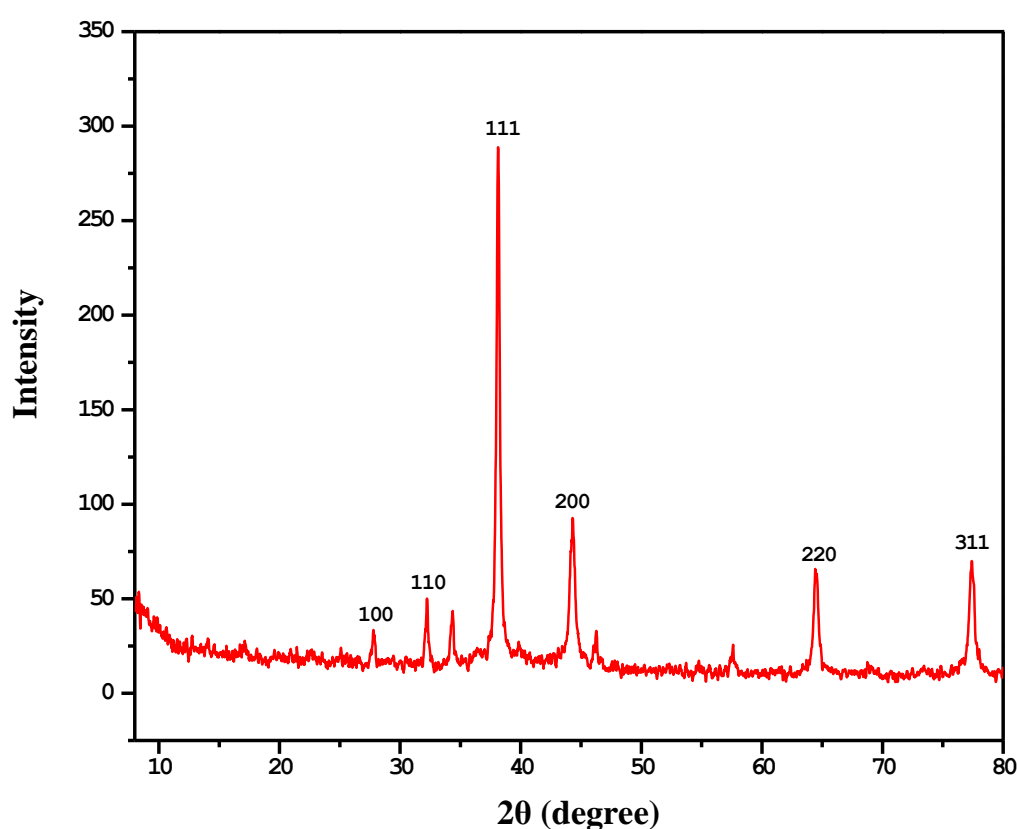


**Figure 3.** XRD spectrum of the synthesized Ag<sub>2</sub>O MPs.

### 2.1.4. SEM-EDX Analyses

Figure 4a,b show the SEM micrograph of Ag<sub>2</sub>O MPs under low and high resolutions. The micrographs indicate irregularly dispersed particles of almost sphere shape with separate limits. The mean particle size, i.e., 0.40 μm (400 nm), was predicted by selecting 100 random features from Figure 4b using Nano Measurer 1.2.5 software. The Ag<sub>2</sub>O particle size distribution ranged from 0.06 μm (60 nm) to 1.87 μm (1870 nm), as displayed in Figure 4c.

The EDX spectrum of silver oxide microparticles is shown in Figure 4d, which represents peaks in the range of 0.0–14.0 keV. The four small peaks at 0.2, 0.4, 0.6, and 0.8 keV indicate the presence of carbon, oxygen, copper, and zinc, respectively. A strong band is allocated to silver at 3 keV. The percentage mass of carbon, oxygen, copper, zinc, and silver predicted in the sample were 12.8, 15.4, 2.5, 2.0, and 66.5, respectively. The presence of carbon, copper, and zinc could be due to the green tea leaves extract.

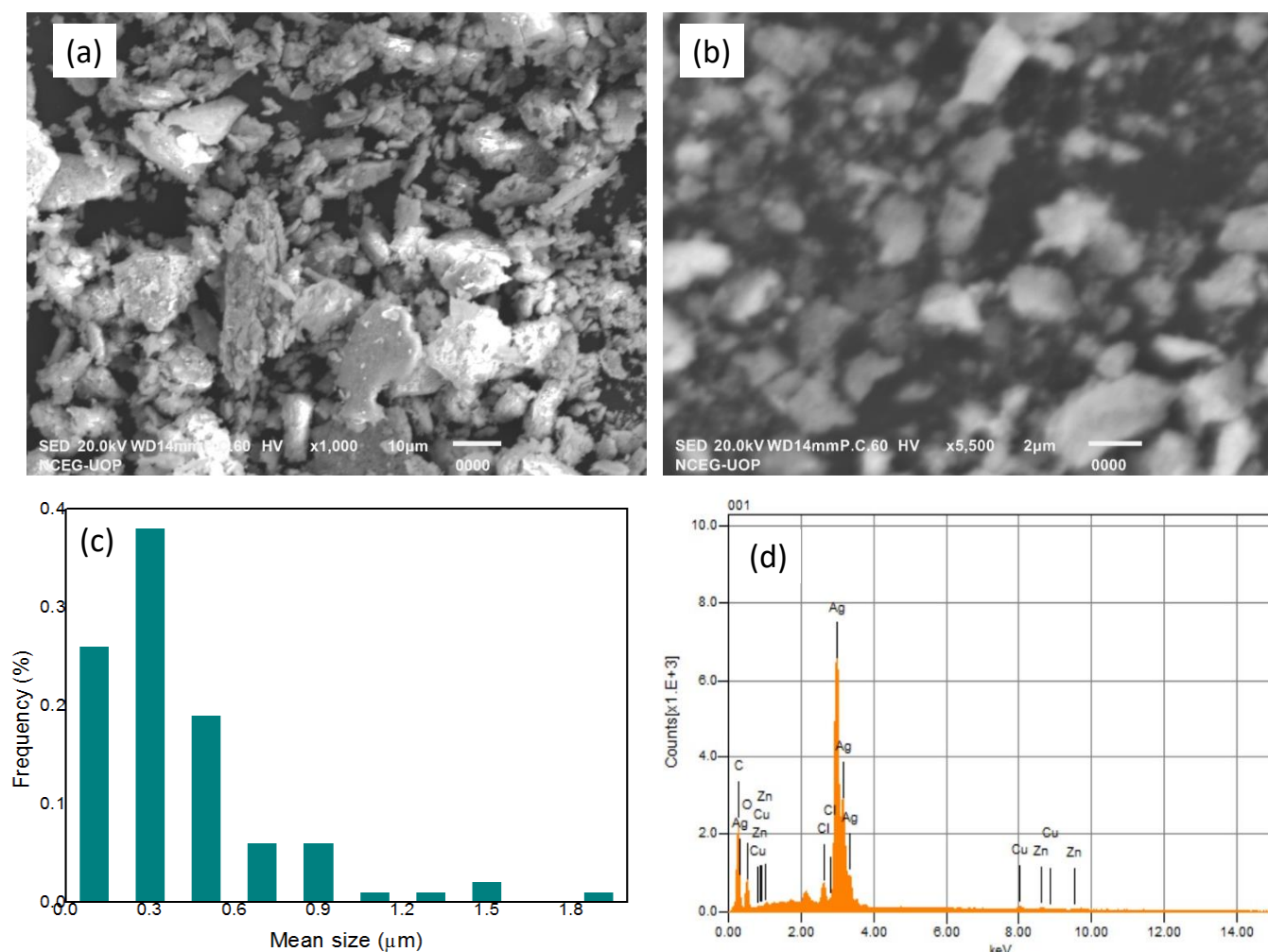


**Figure 4.** (a) and (b). SEM micrograph of  $\text{Ag}_2\text{O}$  microparticles under low and high resolution, respectively. (c) Particle size distribution and (d) EDX spectrum of  $\text{Ag}_2\text{O}$  microparticles.

## 2.2. Degradation of Malachite Green (MG) by $\text{Ag}_2\text{O}$ MPs

The MG solution (0.4 mM) was examined without the addition of a catalyst ( $\text{Ag}_2\text{O}$ ) or oxidant (persulfate) to test the auto/self-degradation in the absence and presence of solar radiation for 3 h at neutral pH. Figure 5a does not demonstrate any significant MG degradation. The degradation of MG by  $\text{Ag}_2\text{O}$  MPs was studied in deionized water at neutral pH and room temperature, i.e.,  $27 \pm 1^\circ\text{C}$ , without introducing sunlight. In order to avoid the interaction of radiation with the reaction mixture, the glass vial that contained the reaction mixture was wrapped in aluminum foil (Figure 5b). An aqueous solution of MG (0.4 mM) was loaded with  $0.1 \text{ g L}^{-1}$  of the synthesized  $\text{Ag}_2\text{O}$  MPs and the time course spectra were recorded (Figure 5b). The MG dye was degraded with the passage of time, and the degradation reaction followed zero-order kinetics with the observed rate constant ( $k_{\text{obs}}$ ),  $2.7 \times 10^{-7} \text{ M min}^{-1}$  (Figure 5c). The slope of the plot yielded  $\epsilon b k_{\text{obs}}$  according to Equation (2) because we monitored absorbance ( $A$ ) as a function of time ( $t$ ). The value of molar absorptivity ( $\epsilon$ ) of MG was determined to be  $2411 \text{ M}^{-1} \text{ cm}^{-1}$  and the path length ( $b$ ) of the quartz cuvette was 1 cm. The degradation of MG is zero-order, corresponding to  $\text{Ag}_2\text{O}$ , because the reaction was studied under the pseudo-first-order condition with excess MG over  $\text{Ag}_2\text{O}$ . Figure 5d shows that about 32.5% MG was degraded by  $\text{Ag}_2\text{O}$  MPs in the absence of solar radiation in 3 h.

$$[A]_t = [A]_0 - \epsilon b k_{\text{obs}} t \quad (2)$$

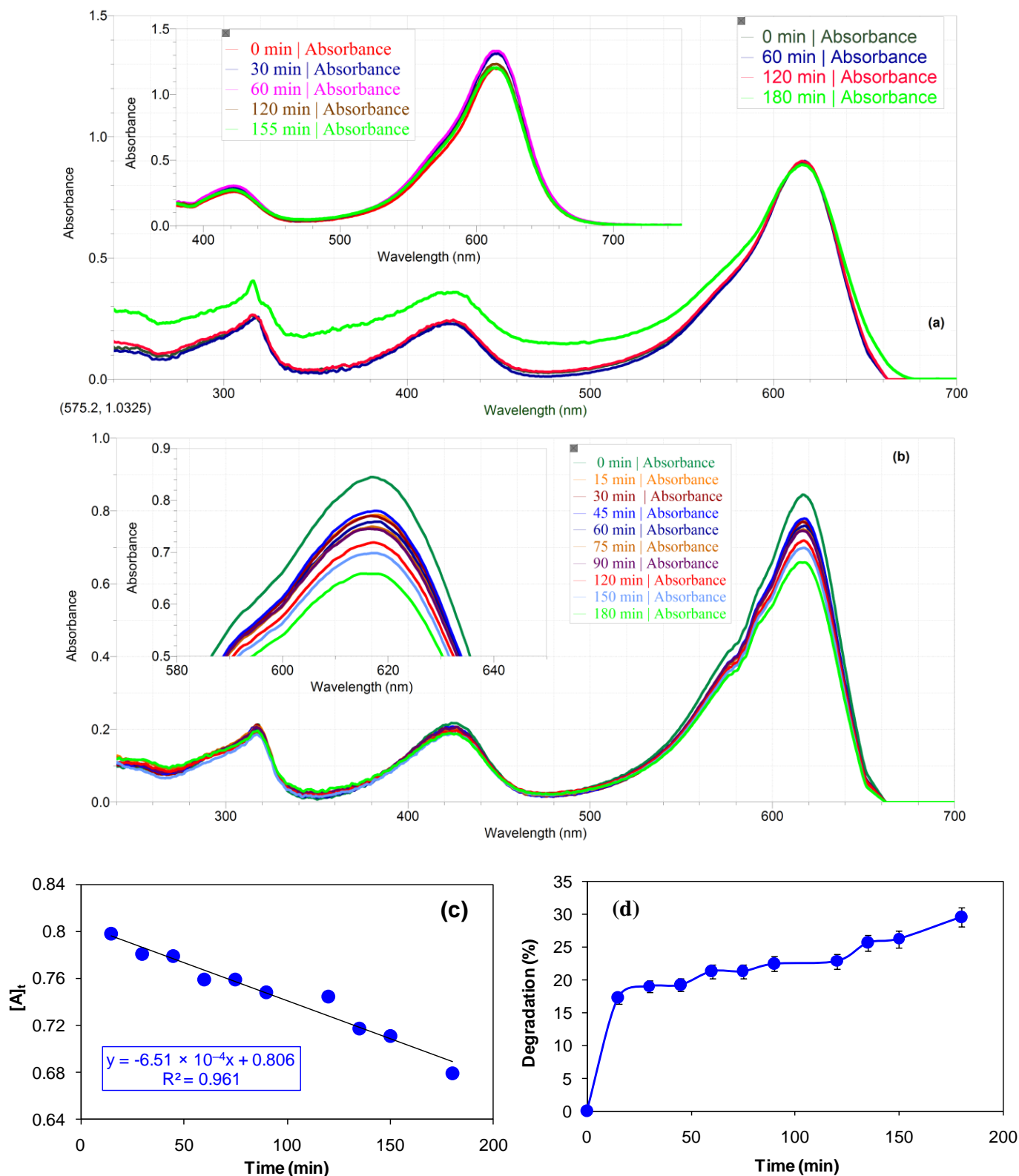


**Figure 5.** (a) Absorption spectra of MG as a function of time in the absence of solar radiation. Inset shows spectra of MG as a function of time in solar radiation. (b) Absorption spectra of the degradation of MG by Ag<sub>2</sub>O MPs in the absence of solar radiation. (c) Plot of the zero-order degradation kinetics in the absence of solar radiation. (d) Degradation of MG by Ag<sub>2</sub>O MPs in the absence of solar radiation.

### 2.3. Photocatalysis of the Degradation of MG by Ag<sub>2</sub>O MPs

Figure 6a shows the spectra of the degradation of MG by solar/Ag<sub>2</sub>O MPs in an aqueous medium as a function of time. An aqueous solution of MG (0.4 mM) was loaded with 0.1 g L<sup>-1</sup> of the synthesized Ag<sub>2</sub>O MPs using a similar procedure as described in Section 2.2. Time course spectra were recorded after exposing the transparent glass vial containing the reaction mixture to direct sunlight, indicating zero-order kinetics corresponding to Ag<sub>2</sub>O MPs and 83% MG degradation in 3 h (Figure 6b,c). The observed rate constant,  $k_{\text{obs}}$ , of the photocatalytic degradation of MG by solar/Ag<sub>2</sub>O was estimated to be  $1.2 \times 10^{-6} \text{ M min}^{-1}$  (Figure 6b). The degradation of malachite green by solar/Ag<sub>2</sub>O photocatalysis was due to the generation of hydroxyl radical (HO<sup>•</sup>), according to Equations (3)–(10) [43]. Wang et al. reported that Ag<sub>2</sub>O is a highly efficient visible light-activated photocatalyst for the degradation of organic contaminants in water [44].

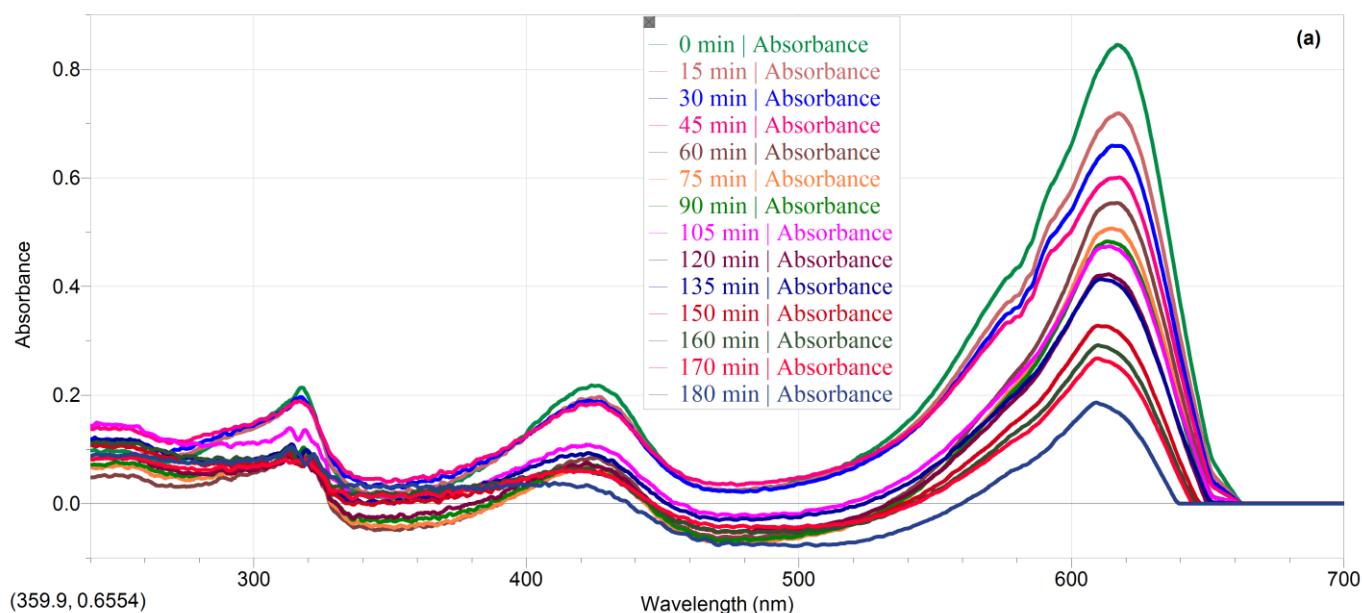
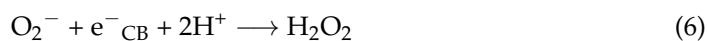
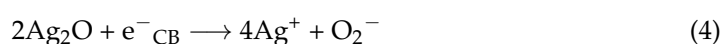
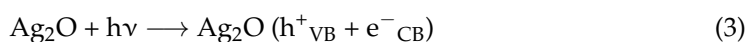
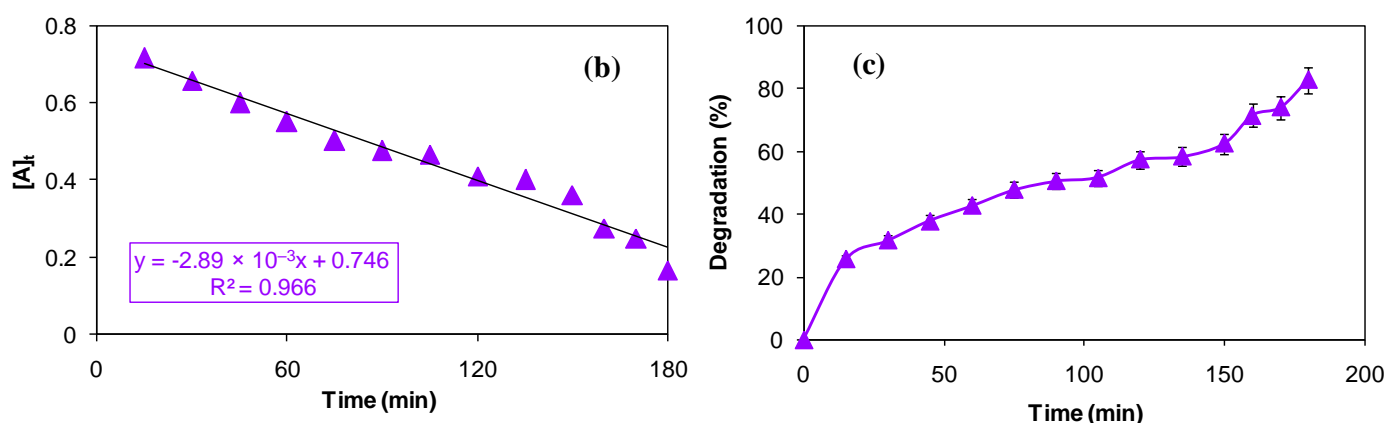


Figure 6. Cont.



**Figure 6.** (a) Absorption spectra of the degradation of MG by Ag<sub>2</sub>O MPs in solar radiation. (b) Plot of the zero-order degradation kinetics. (c) Percent degradation of MG by Ag<sub>2</sub>O MPs in solar radiation.

#### 2.4. Synergistic Effect of Persulfate (PS) on the Degradation of MG by Ag<sub>2</sub>O MPs

Figure 7a,b show the degradation efficiency of Ag<sub>2</sub>O/persulfate system ([PS]<sub>0</sub> = 1.6 mM, [MG]<sub>0</sub> = 0.4 mM, Ag<sub>2</sub>O = 0.1 g L<sup>-1</sup>, pH = 1), represented by the complete removal of MG in water within 21 min in the absence of solar radiations, with the corresponding observed first-order rate constant (*k'*<sub>obs</sub>), i.e., 0.174 min<sup>-1</sup> at room temperature (T = 21 ± 1 °C). The reaction was studied under pseudo-second order condition by keeping PS in excess over MG that was maintained in excess over Ag<sub>2</sub>O. The first-order kinetics was observed with respect to MG. The integration method was applied to the absorbance data that was collected as a function of time to plot a linear graph according to Equation (11). The slope of the plot yielded the observed rate constant (*k'*<sub>obs</sub>), i.e., 0.174 min<sup>-1</sup>. The efficient degradation of MG by the Ag<sub>2</sub>O/PS system was due to the generation of SO<sub>4</sub><sup>•-</sup>, as expressed by Equation (12). Furthermore, additional HO<sup>•</sup> could also be produced due to the reaction of SO<sub>4</sub><sup>•-</sup> with H<sub>2</sub>O, according to Equation (13), which was scavenged by the addition of protons via studying the degradation at pH = 1.

$$\ln[A]_t = \ln[A]_0 - k'_{\text{obs}}t \quad (11)$$

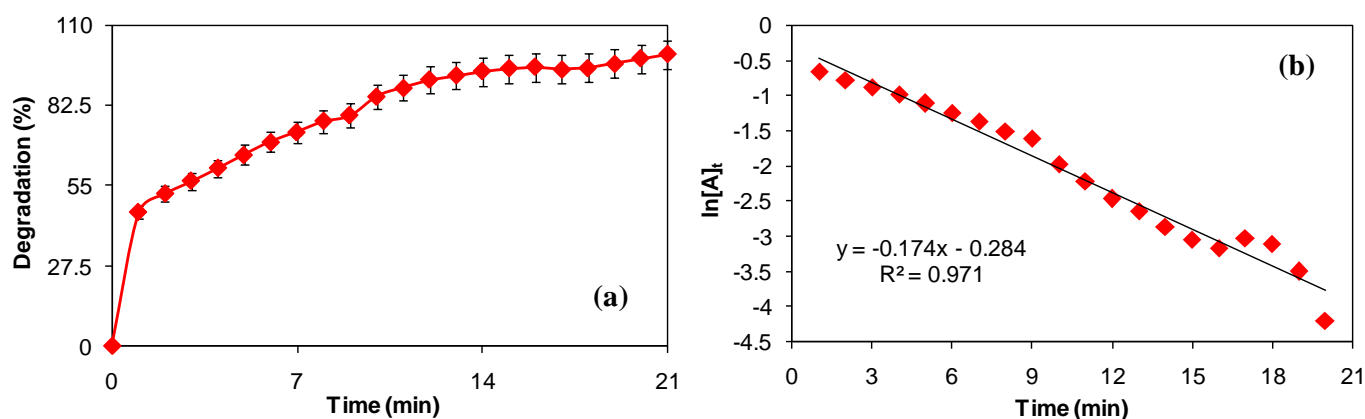


**Figure 7.** (a) Percent degradation of MG by Ag<sub>2</sub>O/PS system at pH = 1. (b) Plot of the first-order degradation kinetics of MG by Ag<sub>2</sub>O/PS system at pH = 1.

The degradation efficiency of the Ag<sub>2</sub>O/PS system was further enhanced under the sunlight, i.e., solar/Ag<sub>2</sub>O/PS, represented by the complete removal of MG in water at pH = 1. The increased efficiency of the Ag<sub>2</sub>O/PS system was demonstrated by a reduction in degradation time of up to 15 min and a high value of the observed first-order rate

constant ( $k'_{\text{obs}}$ ), i.e.,  $0.229 \text{ min}^{-1}$  (Figure 8a–c). A plausible reason could be the generation of more  $\text{SO}_4^{\bullet-}$ , according to Equation (14). However, the increase in acidity could lead to the formation of excess  $\text{SO}_4^{\bullet-}$  on scavenging of hydroxyl radicals by excess protons and yielding water. Saleh et al. reported that the methylene blue (MB) degradation efficiency of  $\text{Ag}_2\text{O}/\text{TiO}_2/\text{nanographene platelet}$  ( $\text{Ag}_2\text{O}/\text{TiO}_2/\text{NGP}$ ) system was enhanced in the presence of  $\text{H}_2\text{O}_2$  and/or PS [45] in water attributed to the same reasons.

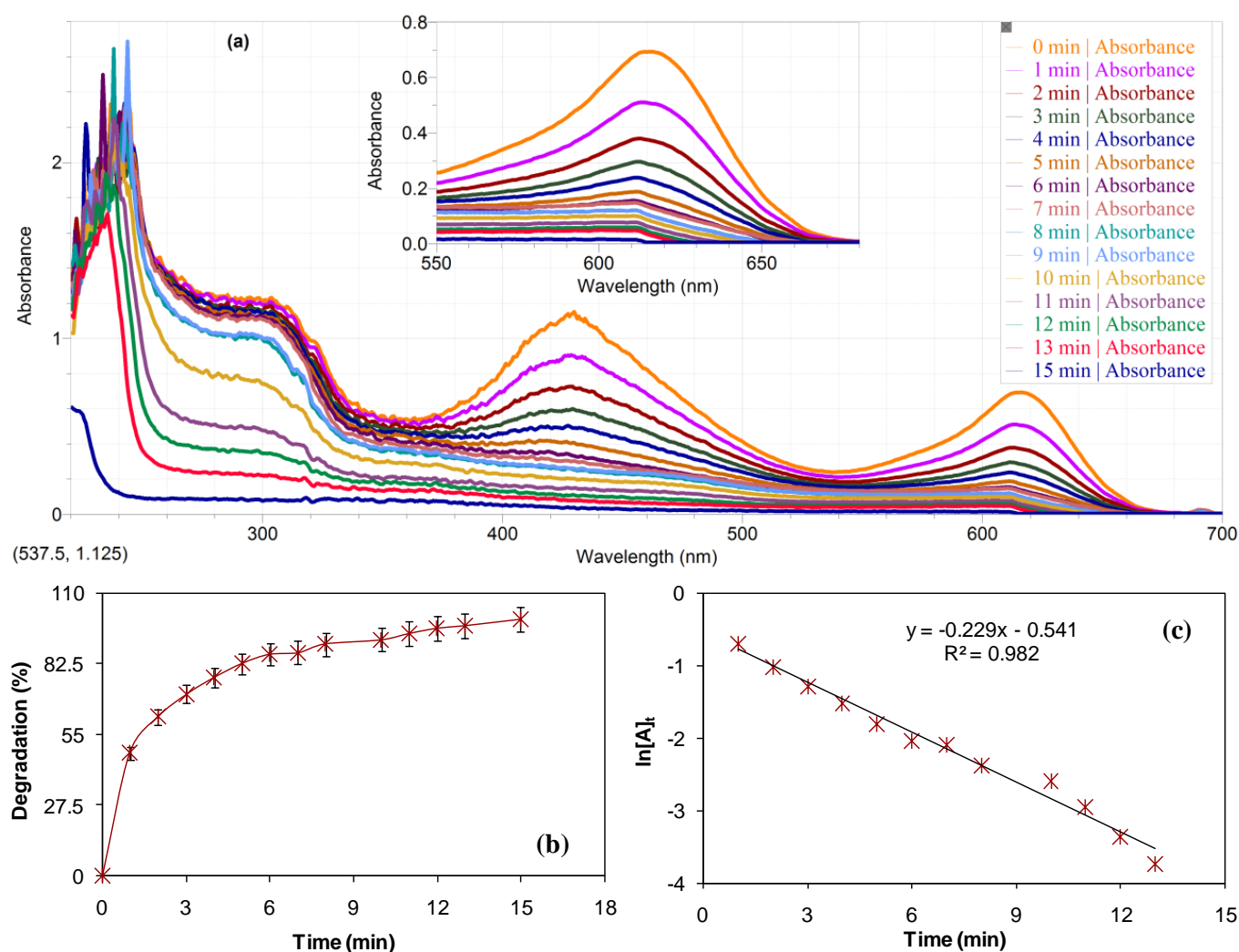
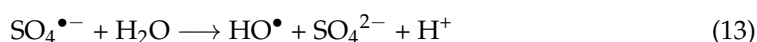


**Figure 8.** (a) Absorption spectra of the degradation of MG by solar/ $\text{Ag}_2\text{O}/\text{PS}$  system at pH = 1. (b) Percent degradation of MG by solar/ $\text{Ag}_2\text{O}/\text{PS}$  system at pH = 1. (c) Plot of the first-order degradation kinetics of MG by solar/ $\text{Ag}_2\text{O}/\text{PS}$  system at pH = 1.

### 2.5. Degradation Kinetics of MG with Respect to the Initial Concentration of MG

The effect of the initial concentration of MG on its degradation kinetics was studied under the pseudo-second-order condition, i.e.,  $\text{PS} \gg \text{MG} \gg \text{Ag}_2\text{O}$ . The concentration of oxidant and catalyst doses such as  $[\text{PS}]_0 = 1.6 \text{ mM}$ , and,  $\text{Ag}_2\text{O} = 0.1 \text{ g L}^{-1}$  were constant at neutral pH and room temperature, i.e.,  $27 \pm 1 \text{ }^\circ\text{C}$ . The initial concentration of MG was varied, such as  $[\text{MG}]_0 = 0.1, 0.2, 0.4, 0.6,$  and  $0.9 \text{ mM}$ . The rate of degradation of MG

was found to show fractional (1/2 or 0.5) order dependence on the concentration of MG according to Equation (15). Consequently, the reaction followed a fractional (1/2) order in MG. Figure 9a–c display zero ( $[A]_t$  vs. time), first ( $\ln[A]_t$  vs. time), and fractional ( $[A]_t^{0.5}$  vs. time) order linear plots, respectively, according to the integration method. The best linear regression fit was observed for the fractional (1/2) order kinetics with  $R^2$  close to 1 (Figure 9c). The fractional order rate constant ( $k''_{\text{obs}}$ ), however, declined with increasing initial MG concentration and became virtually constant at the highest MG concentration with the corresponding rate constant,  $(k''_{\text{obs}})_{\text{max}}$ , as shown in Figure 9d. The rate constant ( $k''_{\text{obs}}$ ) was not significantly affected by further increases in the initial MG concentration. The outcome demonstrates that the slowest rate of MG degradation was found at the highest initial concentration of MG (Figure 9e, i.e., plot of percent degradation vs. time). The reciprocal of the initial MG concentration was plotted against the fractional order rate constant ( $k''_{\text{obs}}$ ) in order to obtain the value of  $(k''_{\text{obs}})_{\text{max}}$ . A plot of  $k''_{\text{obs}}$  versus  $[MG]^{-1}$  yielded a linear fit with  $R^2 = 0.97$  (Figure 9f). The intercept of the plot yields the ideal value of the rate constant, i.e.,  $5.73 \times 10^{-4} \text{ M}^{0.5} \text{ min}^{-1}$  at the infinite concentration of MG that may also refer to the rate constant at the maximum concentration of MG, i.e.,  $(k''_{\text{obs}})_{\text{max}}$ , such as the phase when the rate constant becomes independent of the concentration of dye.

$$[A]_t^{0.5} = [A]_0^{0.5} - 0.5(\epsilon b)^{0.5} k''_{\text{obs}} t \quad (15)$$

## 2.6. Degradation Kinetics of MG with Respect to PS

The effect of variation in PS concentration on the kinetics of MG degradation was examined under the pseudo-second-order condition of  $PS \gg MG \gg Ag_2O$ . The MG concentration and catalyst dose, such as  $[MG]_0 = 0.4 \text{ mM}$  and  $Ag_2O = 0.1 \text{ g L}^{-1}$ , were constant at neutral pH and room temperature ( $27 \pm 1 \text{ }^\circ\text{C}$ ). The initial concentration of PS was varied, such as  $[PS]_0 = 0.8, 1.2, 1.6, 2.0,$  and  $2.4 \text{ mM}$ . The results revealed that the rate of MG degradation has a fractional (0.5) order dependence on the concentration of MG. As a result, the reaction occurred in MG in a fractional order. According to the integration method, Figure 10a–c show zero ( $[A]_t$  vs. time), first ( $\ln[A]_t$  vs. time), and fractional ( $[A]_t^{0.5}$  vs. time) order linear plots, respectively. For the fractional order kinetics, a linear regression fit with an  $R^2$  close to 1 was found to be the best (Figure 10c). However, the fractional order rate constant rose linearly with increasing initial PS concentration, revealing first order in PS, and the negative value of the intercept indicates that MG is degrading independently of PS by the catalyst  $Ag_2O$  as was discussed in Sections 2.2 and 2.3 (Figure 10d). According to Equations (16–18), the slope of the plot results in the overall fractional (3/2) order degradation rate constant ( $k = 0.794 \text{ M}^{-0.5} \text{ min}^{-1}$ ), as seen in Figure 10d.

$$\text{Rate} = k[MG]^{0.5}[PS][Ag_2O]^0 \quad (16)$$

We can say that the pseudo-second-order condition was kept by keeping PS in excess over MG, which was kept in excess over  $Ag_2O$ . Equation (16) is therefore simplified to Equation (17).

$$\text{Rate} = k''_{\text{obs}}[MG]^{0.5} \quad (17)$$

Since,

$$k''_{\text{obs}} = k[PS] \quad (18)$$

However, Figure 10d demonstrates that an outlayered value of the observed fractional order rate constant ( $k''_{\text{obs}}$ ) is attained when the concentration of PS is 0.8 mM, which is only two-fold the concentration of MG. As a result, it has been declared that the just-doubled PS concentration to MG concentration does not satisfy the pseudo-second-order condition. In order to maintain the pseudo-order condition, the concentration of PS should be in excess of the concentration of MG. However, Figure 10e represents the degradation kinetics of MG as a function of time at a varying concentration of PS.

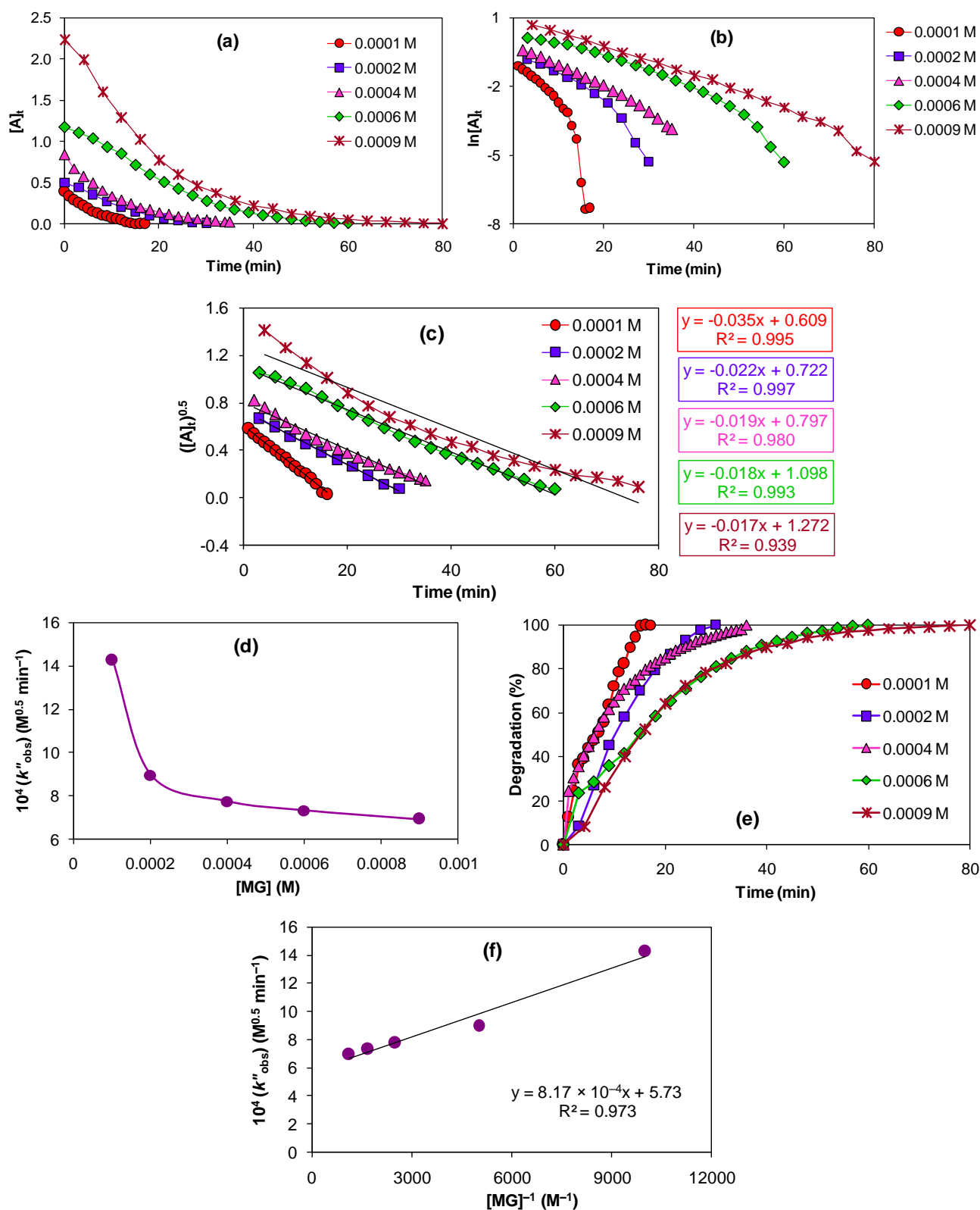


**Figure 9.** Kinetic study of the degradation of MG corresponding to the initial dye concentration at neutral pH, 1.6 mM PS, 0.1 g L<sup>-1</sup> Ag<sub>2</sub>O, and 27 ± 1 °C. (a) Zero-order plot. (b) First-order plot. (c) Fractional (0.5) order plot. (d) Plot of fractional-order rate constant versus [MG]. (e) Plot of percent degradation of MG as a function of time at a varying concentration of MG. (f) Plot of the fractional-order rate constant versus reciprocal of [MG].

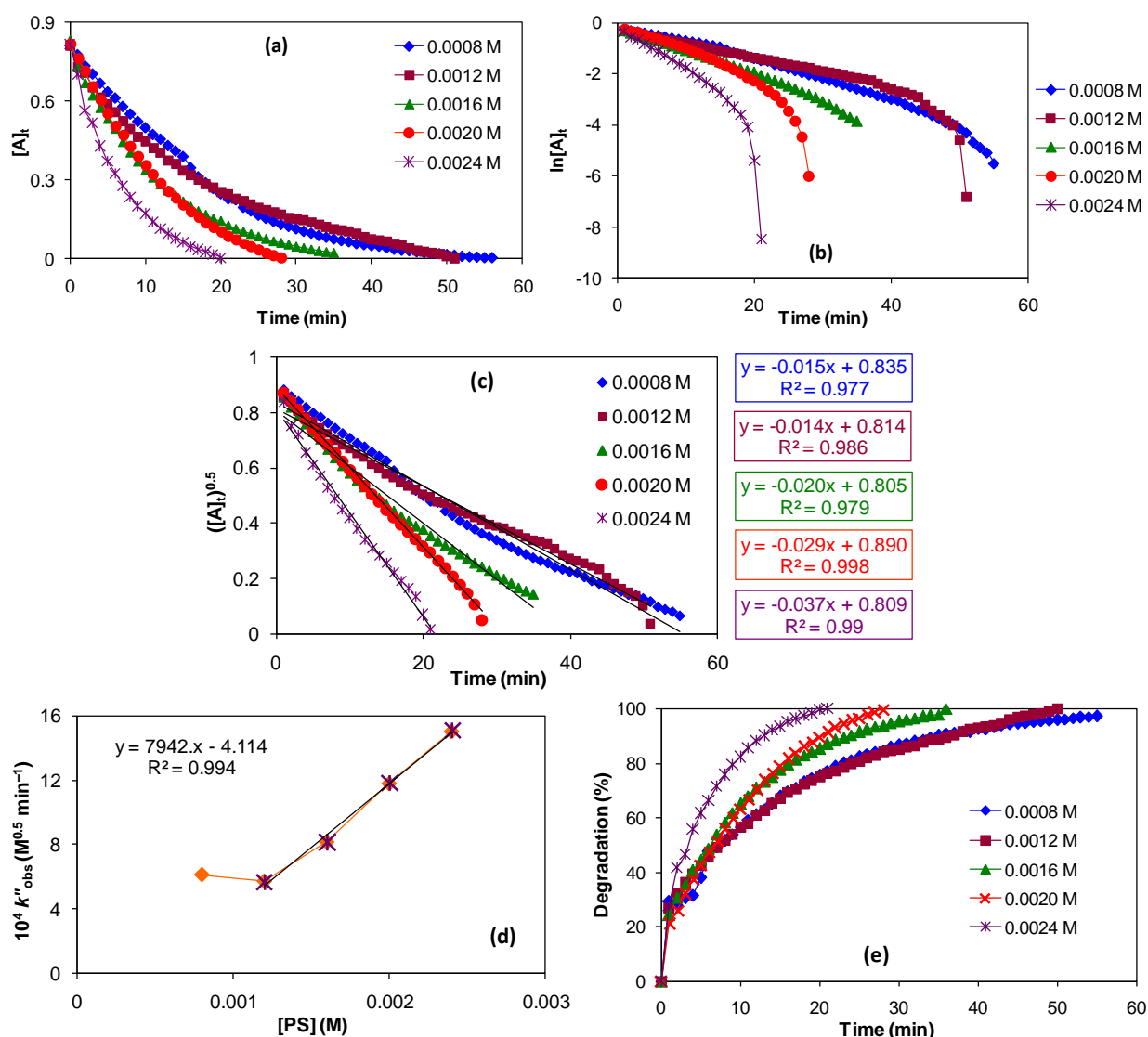


**Figure 10.** Kinetic study of the degradation of MG corresponding to PS concentration at neutral pH, 0.4 mM MG,  $0.1 \text{ g L}^{-1} \text{Ag}_2\text{O}$ , and  $27 \pm 1 \text{ }^\circ\text{C}$ . (a) Zero-order plot. (b) First-order plot. (c) Fractional (0.5) order plot. (d) Plot of fractional-order rate constant versus  $[\text{PS}]$ . (e) Plot of percent degradation of MG as a function of time at a varying concentration of PS.

### 2.7. Effect of pH on the Degradation Kinetics of MG

The degradation of MG was studied at various pH levels, including acidic, neutral, and basic. The reaction was studied under the pseudo-second-order condition, i.e.,  $\text{PS} \gg \text{MG} \gg \text{Ag}_2\text{O}$ . Except for pH, the experimental conditions such as  $[\text{MG}]_0 = 0.4 \text{ mM}$ ,  $[\text{PS}]_0 = 1.6 \text{ mM}$ , and  $\text{Ag}_2\text{O} = 0.1 \text{ g L}^{-1}$  were kept constant at  $27 \pm 1 \text{ }^\circ\text{C}$ . To study the effect of pH on the degradation of MG, pH levels of 1, 3, 5, 7, and 8 were varied. Figure 11a–f reveal the effect of pHs on the degradation kinetics of MG. In acidic pHs of 1, 3, and 5, the MG degradation reaction followed a first-order kinetics corresponding to MG (Figure 11c). However, at neutral and basic pHs of 7 and 8, respectively, MG degradation occurred in the usual fractional order (Figure 11b). The results also show a linear relationship between the observed first-order rate constant ( $k'_{\text{obs}}$ ) and the reciprocal of pHs in the acidic range, with the best linear regression  $R^2$  value near 1 (Figure 11f). The results helped to conclude that the formation of hydroxyl radical (Equation (13)) is reduced during the reaction in an acidic medium by yielding water, and thus the degradation is accelerated by the synergistic effect of PS ion. As a result, the reaction order with respect to MG concentration is raised

to first from fractional (1/2) order. The rate of percent degradation of MG shows the following decreasing order with reference to pH of the solution. Because of the scavenging of hydroxyl radical by free protons and hydroxyl ion at pHs 1 and 8, degradation was rapid. It is worth noting that a minimum 1 M nitric acid solution acts as an oxidizing agent; we used a 0.1 M solution to maintain pH [46].

$$1 > 8 > 3 > 5 > 7$$

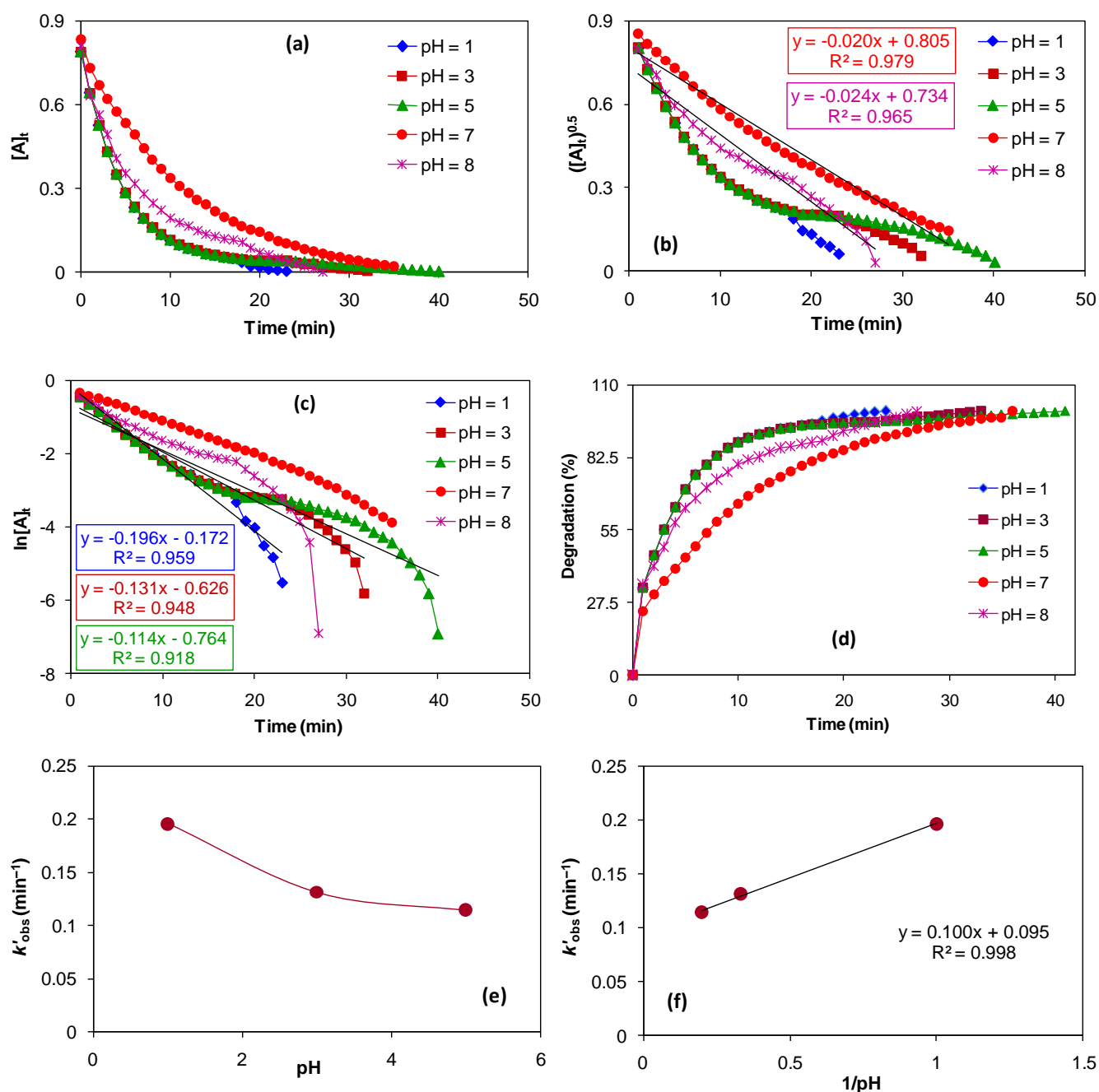


**Figure 11.** Effect of pH on the degradation of MG. (a) Zero-order plot. (b) Fractional (0.5) order plot. (c) First-order plot. (d) Plot of percent degradation of MG as a function of time at varying pH. (e) Plot of first-order rate constant versus pH. (f) Plot of first-order rate constant versus reciprocal of pH.

### 2.8. Reusability of Ag<sub>2</sub>O MPs

The reusability of Ag<sub>2</sub>O MPs was tested over four cycles by keeping reaction parameters constant such as [PS]<sub>0</sub> = 1.6 mM, [MG]<sub>0</sub> = 0.4 mM, Ag<sub>2</sub>O = 0.1 g L<sup>-1</sup>, and 27 ± 1 °C at neutral pH. Following filtration of the first and subsequent used solution, the Ag<sub>2</sub>O MPs were collected on filter paper and washed with deionized water, dried, and reused. The catalyst performs admirably, beginning with 100% degradation in the first use and progressing to 97.3% degradation in the third and fourth uses. This minor variation in catalyst efficiency may be encountered by using the catalyst again after collecting from filter paper, which may result in a minor weight loss of the catalyst at the filter paper. Meanwhile, in the first use, the MG degradation kinetics followed fractional order as expected, but from the second to fourth use, it went through first order, possibly due to surface changes in the catalyst (Figure 12a–c). From the first to the fourth use, the degradation rate of MG was gradually reduced may because of the weight loss, as mentioned earlier. The results are depicted in Figure 12d,e.

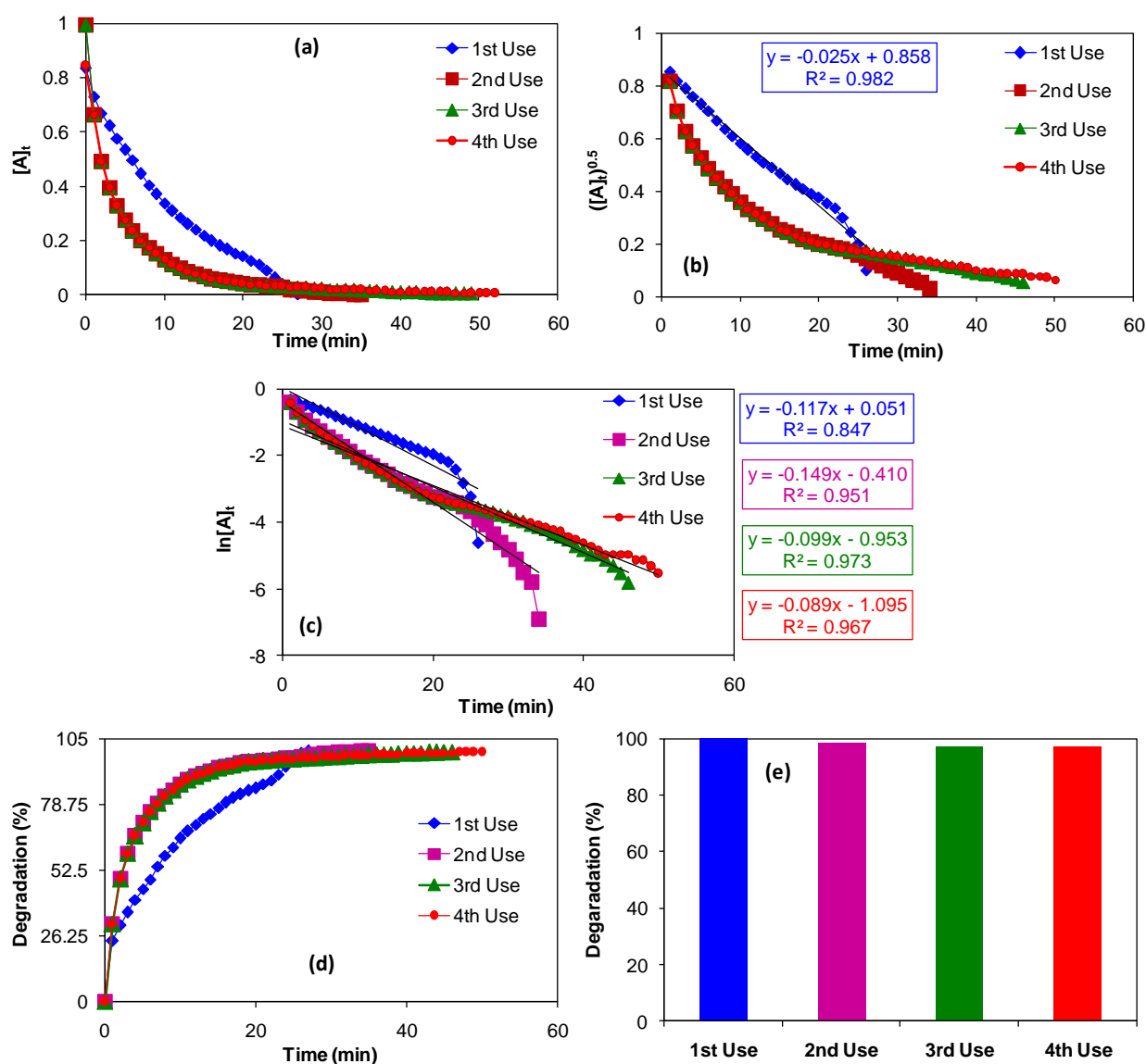


**Figure 12.** Reusability of the catalyst Ag<sub>2</sub>O MPs at neutral pH with constant experimental conditions of [PS]<sub>0</sub> = 1.6 mM, [MG]<sub>0</sub> = 0.4 mM, Ag<sub>2</sub>O = 0.1 g L<sup>-1</sup>, and 27 ± 1 °C. (a) Zero-order plot. (b) Fractional (0.5) order plot. (c) First-order plot. (d) Plot of percent degradation of MG as a function of time in reusability cycles. (e) Percent degradation of MG in reusability cycles.

### 2.9. Comparative Study of the PS Activation by Iron(II) Sulfate and Its Effect on the Degradation of MG

At  $0.2 \text{ g L}^{-1}$  of the catalyst, i.e., iron(II) sulfate in  $0.4 \text{ mM}$  aqueous solution of MG and  $1.6 \text{ mM}$  PS, a comparative examination of the PS activation by iron(II) sulfate rather than silver oxide was conducted in room temperature ( $26 \pm 1 \text{ }^\circ\text{C}$ ) at neutral pH. Figure 13a,b show that the rate of MG degradation in the  $\text{FeSO}_4/\text{PS}$  system was lower than that in the  $\text{Ag}_2\text{O}/\text{PS}$  system.  $\text{Ag}_2\text{O}/\text{PS}$  system completely degraded MG in 36 min, which is about >2 times faster than the  $\text{FeSO}_4/\text{PS}$  system, which demonstrated 99.3% degradation of MG in 79 min. A comparison of the degradation of MG under various experimental circumstances is shown in Table 1.

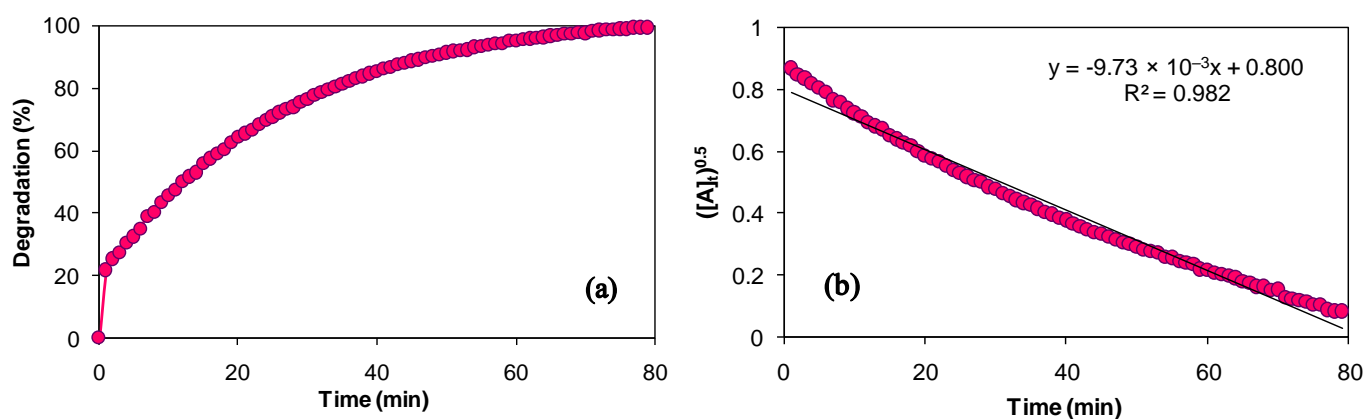


**Figure 13.** (a) Percent degradation of MG by  $\text{FeSO}_4/\text{PS}$  system at neutral pH and room temperature. (b) Plot of the fractional-order degradation kinetics of MG by  $\text{FeSO}_4/\text{PS}$  system at neutral pH and room temperature.

**Table 1.** Comparative analysis of the degradation of MG under different experimental conditions.

Experimental Conditions at Room Temperature	Percent Degradation (Time in Minute)
$0.4 \text{ mM MG}/0.1 \text{ g L}^{-1} \text{ Ag}_2\text{O}/\text{pH}(\text{neutral})/\text{dark}$	32.5 (180)
$0.4 \text{ mM MG}/0.1 \text{ g L}^{-1} \text{ Ag}_2\text{O}/\text{pH}(\text{neutral})/\text{sunlight}$	83 (180)
$0.4 \text{ mM MG}/0.1 \text{ g L}^{-1} \text{ Ag}_2\text{O}/1.6 \text{ mM PS}/\text{pH}(1)/\text{without sunlight}$	100 (21)
$0.4 \text{ mM MG}/0.1 \text{ g L}^{-1} \text{ Ag}_2\text{O}/1.6 \text{ mM PS}/\text{pH}(1)/\text{sunlight}$	100 (15)
$0.4 \text{ mM MG}/0.1 \text{ g L}^{-1} \text{ Ag}_2\text{O}/1.6 \text{ mM PS}/\text{pH}(\text{neutral})/\text{without sunlight}$	100 (36)
$0.4 \text{ mM MG}/0.1 \text{ g L}^{-1} \text{ Ag}_2\text{O}/1.6 \text{ mM PS}/\text{pH}(8)/\text{without sunlight}$	99.9 (27)
$0.4 \text{ mM MG}/0.2 \text{ g L}^{-1} \text{ FeSO}_4/1.6 \text{ mM PS}/\text{pH}(\text{neutral})/\text{without sunlight}$	99.3 (79)

### 2.10. Proposed Degradation Mechanism of MG

According to Equations (3)–(10), the hydroxyl radical produced by the photo-excitation of the electron from the valence band to the conduction band of silver oxide plays a leading role in the degradation of MG dye. This electron reacts with oxygen to form the hydroxyl radical, which degrades MG in an aqueous solution (Equations (5)–(9)). In the absence of sunlight, however, the minor change in the concentration of MG could be due to MG adsorption on the surface of  $\text{Ag}_2\text{O}$  MPs. Another mode of degradation in the presence of sunlight could be the role of MG as a photosensitizer after adsorption on the surface of  $\text{Ag}_2\text{O}$  MPs. The surface-adsorbed MG is excited and donates an electron to the conduction band of  $\text{Ag}_2\text{O}$  MPs by absorbing solar light. These electrons were scavenged by the surface-adsorbed  $\text{O}_2$  and reacted with surface-adsorbed  $\text{H}_2\text{O}$  to form  $\text{H}_2\text{O}_2$ , which then produces hydroxyl radicals and degrades the surface-adsorbed MG dye. When a dye molecule degrades, another dye molecule is adsorbed on the surface of  $\text{Ag}_2\text{O}$  MPs, restarting the

photocatalytic cycle [47]. Meanwhile, the synergistic effect of persulfate may follow the mechanism of photo-excitation of  $\text{Ag}_2\text{O}$  and generation of  $\text{SO}_4^{\bullet-}$  radical according to Equations ((3)–(6), (12)–(14)), which helps to completely degrade the MG dye as seen in the spectrum (Figure 8a). We see no significant peak in the UV-visible region after 15 min. Figures 6a and 8a show a difference in the intensity of the  $\pi$ – $\pi^*$  transition in the MG absorption spectrum because of different degradation mechanisms and scavenging of hydroxyl radicals by the high concentration of protons at  $\text{pH} = 1$ .

### 3. Materials and Methods

#### 3.1. Materials

Dried green tea leaves (*Camellia sinensis*) were purchased from a local market in Peshawar, Pakistan. Analytical grade sodium dodecyl sulfate (SDS) ( $\text{CH}_3(\text{CH}_2)_{11}\text{OSO}_3\text{Na}$ ), sodium persulfate (PS) ( $\text{Na}_2\text{S}_2\text{O}_8$ ), iron(II) sulfate heptahydrate ( $\text{FeSO}_4 \cdot 7\text{H}_2\text{O}$ ), malachite green oxalate salt ( $\text{C}_{23}\text{H}_{25}\text{N}_2 \cdot \text{C}_2\text{HO}_4 \cdot 0.5\text{C}_2\text{H}_2\text{O}_4$ ), and silver nitrate ( $\text{AgNO}_3$ ) were purchased from Sigma-Aldrich (St. Louis, MO, USA). The  $\text{AgNO}_3$  was used as a pioneer salt for the synthesis of silver oxide ( $\text{Ag}_2\text{O}$ ) microparticles, while green tea was used as a reducing and stabilizing agent. The pH of the solution was adjusted by using 0.1 M  $\text{HNO}_3$  (Merck, 67% extra pure) and KOH (Sigma-Aldrich). Deionized water was used for the preparation of all solutions. All the chemicals were used as received.

#### 3.2. Green Tea Leaves Processing

About 7.4 g of green tea (GT) leaves powder was introduced into a beaker containing 100 mL deionized water and stirred gently for 20 min at 70 °C. The solution was left for 2 h (at room temperature, i.e.,  $25 \pm 1$  °C), and the undissolved matter was separated out. The green tea leaves extract was filtered using Whatman filter paper, and the solution was stored at 5 °C for further use (Figure 14).

#### 3.3. Synthesis of Silver Oxide Microparticles ( $\text{Ag}_2\text{O}$ MPs)

The synthesis of silver oxide microparticles was carried out according to the cited procedure [39]. Briefly, 5 mL of the green tea leaves extract was added to 2 mM (100 mL)  $\text{AgNO}_3$  solution after the addition of 0.0015 g SDS. To stabilize the  $\text{Ag}_2\text{O}$  MPs, SDS was added to the reaction mixture. The resulting mixture was stirred for 2.5 h at 40 °C in the dark. The subsequent precipitate was separated by centrifugation at 8000 rpm for 30 min, followed by washing with deionized water. The resulting dark brown pellet of  $\text{Ag}_2\text{O}$  MPs was dried in a petri dish at 90 °C in oven and stored in an air-tight glass vial (Figure 14).

#### 3.4. Characterization Techniques

The optical properties of the synthesized  $\text{Ag}_2\text{O}$  MPs were studied by a UV-visible spectrophotometer (UV-1800, Shimadzu, Kyoto, Japan) in the wavelength range of 400–800 nm. The crystallinity of  $\text{Ag}_2\text{O}$  MPs was determined by X-ray diffraction (XRD) (Malvern Panalytical, Malvern, UK). The functional groups present in the  $\text{Ag}_2\text{O}$  MPs were investigated by Fourier transform infrared (FTIR) spectrophotometer (Shimadzu IR Prestige-21, Duisburg, Germany), using molecular and atomic vibration in the 400 to 4000  $\text{cm}^{-1}$  region. The morphology and composition of  $\text{Ag}_2\text{O}$  microparticles were studied by using a scanning electron microscope (SEM) (TESCAN Vega 3, Brno, Czech Republic) and energy dispersive X-ray (EDX) spectroscopy (Vario EL CHNS, Elementar Analysensysteme GmbH, Hanau, Germany), respectively.

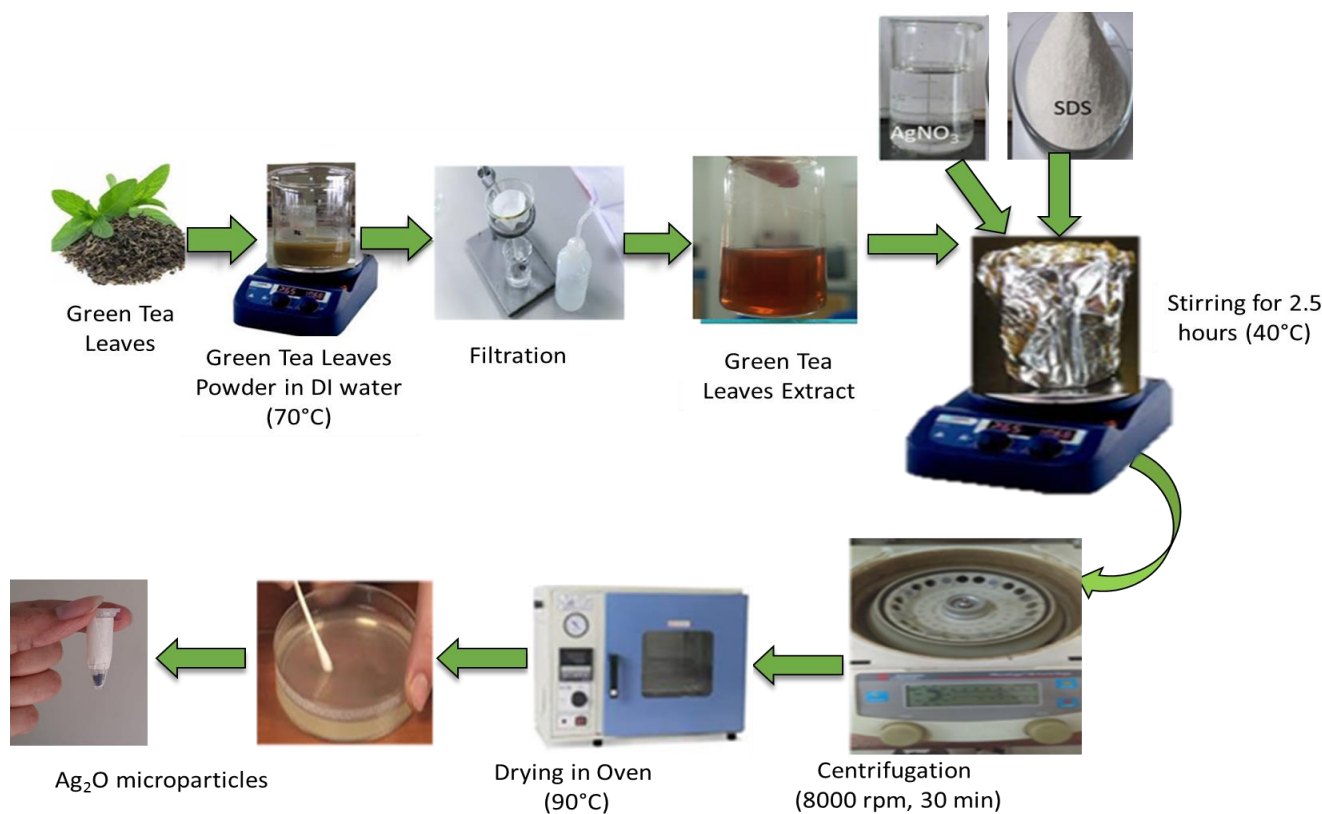


**Figure 14.** Preparation of green tea leaves extract and synthesis of silver oxide microparticles.

### 3.5. Degradation Experiments

The degradation of malachite green was studied in deionized water on a lab scale using a transparent glass vial as a photoreactor and sunlight as a photo/light source. A typical experimental setup includes 10 mL of the dye solution in the transparent glass vial that was loaded with 1 mg of  $\text{Ag}_2\text{O}$  MPs to reveal their catalytic and photocatalytic effect on MG degradation. To investigate the effect of solar light on the degradation of MG without/after introducing  $\text{Ag}_2\text{O}$  MPs, the vial was left in the sun for three hours without being stirred in each case. In the case of the MG degradation study in the dark, the vial was wrapped in aluminum foil without/after introducing  $\text{Ag}_2\text{O}$  MPs and left for 3 h without stirring in both cases. A 3 mL solution was taken at specific time intervals and analyzed by UV/Visible spectrophotometer to record the absorption spectra of MG. Following the spectral analysis, the solution was transferred back to the vial from the cuvette. The typical formulation was used to calculate percent degradation in such a way that the concentration of MG at any specific time point  $t$  ( $C_t$ ) was subtracted from the initial concentration of MG at zero time point ( $C_0$ ) before introducing solar radiation/catalyst. The result was divided by the initial concentration of MG at zero time point ( $C_0$ ), and the result was multiplied by 100 to yield percent MG degradation as follows:  $[(C_0 - C_t)/C_0] \times 100$ . However, the concentration of MG was calculated using the Beer–Lambert law at the selected wavelength of MG, i.e., the maximum wavelength of MG in the visible region (617 nm). The concentration of MG was calculated by dividing the absorbance of MG by the molar absorptivity of MG at 617 nm ( $2411 \text{ M}^{-1} \text{ cm}^{-1}$ ) in a quartz cuvette with a 1 cm path length. Meanwhile, for kinetic analysis, absorbance was plotted directly without conversion to concentration using the integration method and its formulations for different kinetic orders, as detailed in Section 2. The typical experimental step for the synergistic effect of persulfate ion contained persulfate concentration within the overall 10 mL solution of MG and 1 mg of  $\text{Ag}_2\text{O}$  MPs. The kinetic study was conducted on the spectrophotometer's spectrum mode with overlay or kinetic mode with a time interval of at

least 1 min or more to observe the rate of degradation by measuring changes in absorbance as a function of time.

#### 4. Conclusions

Silver oxide microparticles were successfully synthesized by using green tea leaf extract, which is an environmentally friendly and cost-effective method as compared to conventional chemical and physical methods. The FTIR and UV-visible spectroscopy helped to identify the characteristic peaks of Ag<sub>2</sub>O MPs, while the morphology, size, and percent composition of Ag<sub>2</sub>O MPs were explained by SEM, XRD, and EDX analysis, respectively. The mean particle size, i.e., 0.40 μm (400 nm), and the crystallite size, i.e., 7.95 nm of the synthesized Ag<sub>2</sub>O MPs were determined by SEM and XRD, respectively, indicating approximately 50 times smaller size for the crystallite than the particle. The solar photocatalytic degradation of MG using Ag<sub>2</sub>O MPs was 83% during 180 min. Interestingly, Ag<sub>2</sub>O/PS system showed excellent efficiency in removing MG from water, represented by the complete removal of MG in 36 min at neutral pH and 21 min at pH = 1 ([PS]<sub>0</sub> = 1.6 mM), with the corresponding rate constant of 0.174 min<sup>-1</sup> without introducing sunlight. The degradation efficiency of the Ag<sub>2</sub>O/PS system was further increased in the presence of sunlight, represented by complete MG degradation in 15 min with the rate constant of 0.229 min<sup>-1</sup> when the pH of the solution was 1 (i.e., 1.3 times rise). The results revealed that solar/Ag<sub>2</sub>O, particularly solar/Ag<sub>2</sub>O/PS photocatalysis is a promising method for the elimination of toxic organic pollutants, such as malachite green, from the water environment.

**Author Contributions:** Conceptualization, I., R.K. and B.B.; methodology, I., R.K. and B.B.; software, I., R.K., B.B., R.A.Q., H.G., and M.S.K.; validation, S.K., N.B., C.H., and N.U.R.; formal analysis, I., R.K., B.B., R.A.Q., H.G., N.B., and M.S.K.; investigation, I., R.K., B.B., and M.S.K.; resources, I., R.K., B.B., and C.H.; data curation, R.A.Q., H.G., S.K., N.B., and N.U.R.; writing—original draft preparation, I., R.K., and B.B.; writing—review and editing, R.K., B.B., S.K., and C.H.; visualization, R.K. and B.B.; supervision, R.K. and B.B.; project administration, R.K.; funding acquisition, R.K. All authors have read and agreed to the published version of the manuscript.

**Funding:** This research received no external funding.

**Data Availability Statement:** Not applicable.

**Acknowledgments:** Rozina Khattak and Bushra Begum acknowledge the financial and technical support of the Shaheed Benazir Bhutto Women University, Peshawar, Pakistan, and Changseok Han acknowledges the support of the National Research Foundation of Korea (NRF) grant funded by the Korean government (MSIT) (No. 2021R1A2C1093183) and (No. 2021R1A4A1032746).

**Conflicts of Interest:** The authors declare no conflict of interest.

#### References

1. Lee, Y.-C.; Kim, J.-Y.; Shin, H.-J. Removal of malachite green (MG) from aqueous solutions by adsorption, precipitation, and alkaline fading using talc. *Sep. Sci. Technol.* **2013**, *48*, 1093–1101. [[CrossRef](#)]
2. Parshetti, G.; Kalme, S.; Saratale, G.; Govindwar, S. Biodegradation of malachite green by *Kocuria rosea* MTCC 1532. *Acta Chim. Slov.* **2006**, *53*, 492–498.
3. Ali, H.; Ahmad, W.; Haq, T. Decolorization and degradation of malachite green by *Aspergillus flavus* and *Alternaria solani*. *Afr. J. Biotechnol.* **2009**, *8*, 1574–1576.
4. Weng, Y.; Li, J.; Ding, X.; Wang, B.; Dai, S.; Zhou, Y.; Pang, R.; Zhao, Y.; Xu, H.; Tian, B. Functionalized gold and silver bimetallic nanoparticles using *Deinococcus radiodurans* protein extract mediate degradation of toxic dye malachite green. *Int. J. Nanomed.* **2020**, *15*, 1823. [[CrossRef](#)] [[PubMed](#)]
5. Wu, J.; Li, B.; Shao, Y.; Wu, X.; Zhao, W. Piezoelectricity enhances MoSe<sub>2</sub> nanoflowers adsorption of the antibacterial dye malachite green under sonication. *Environ. Chem. Lett.* **2020**, *18*, 2141–2148. [[CrossRef](#)]
6. Daneshvar, N.; Khataee, A.; Rasoulifard, M.; Pourhassan, M. Biodegradation of dye solution containing malachite green: Optimization of effective parameters using Taguchi method. *J. Hazard. Mater.* **2007**, *143*, 214–219. [[CrossRef](#)]
7. Srivastava, S.; Sinha, R.; Roy, D. Toxicological effects of malachite green. *Aquat. Toxicol.* **2004**, *66*, 319–329. [[CrossRef](#)]
8. Sultana, S.; Rehan, K.; Rehan, I.; Ali, F.; Waris, S.; Zahoor, M.; Salman, S.M.; Khan, S.; Rehan, M.S. Physicochemical and instrumental characterization of rice husk and its potential use as a low cost adsorbent for mutagenic dye bromophenol blue. *Z. Phys. Chem.* **2021**, *235*, 1263–1277. [[CrossRef](#)]

9. El-Desouky, N.; Shoueir, K.; El-Mehasseb, I.; El-Kemary, M. Synthesis of silver nanoparticles using bio valorization coffee waste extract: Photocatalytic flow-rate performance, antibacterial activity, and electrochemical investigation. *Biomass Convers. Biorefinery* **2022**, 1–15. [[CrossRef](#)]
10. Vignesh, A.; Manigundan, K.; Santhoshkumar, J.; Shanmugasundaram, T.; Gopikrishnan, V.; Radhakrishnan, M.; Joseph, J.; Ayyasamy, P.M.; Kumar, G.D.; Meganathan, R. Microbial degradation, spectral analysis and toxicological assessment of malachite green by *Streptomyces chrestomycticus* S20. *Bioprocess Biosyst. Eng.* **2020**, *43*, 1457–1468. [[CrossRef](#)]
11. Bethi, B.; Sonawane, S.H.; Bhanvase, B.A.; Mittal, V.; Ashokkumar, M. Sonochemical Synthesis of Go-ZnO Nanophotocatalyst for the Degradation of Malachite Green Using a Hybrid Advanced Oxidation Process. *Nanomaterials* **2019**, *1*, 159–184.
12. Navarro, P.; Zapata, J.P.; Gotor, G.; Gonzalez-Olmos, R.; Gómez-López, V.M. Degradation of malachite green by a pulsed light/H<sub>2</sub>O<sub>2</sub> process. *Water Sci. Technol.* **2019**, *79*, 260–269. [[CrossRef](#)]
13. Berberidou, C.; Poullos, I.; Xekoukoulotakis, N.; Mantzavinos, D. Sonolytic, photocatalytic and sonophotocatalytic degradation of malachite green in aqueous solutions. *Appl. Catal. B Environ.* **2007**, *74*, 63–72. [[CrossRef](#)]
14. Khan, S.; Han, C.; Sayed, M.; Sohail, M.; Jan, S.; Sultana, S.; Khan, H.M.; Dionysiou, D.D. Exhaustive photocatalytic lindane degradation by combined simulated solar light-activated nanocrystalline TiO<sub>2</sub> and inorganic oxidants. *Catalysts* **2019**, *9*, 425. [[CrossRef](#)]
15. Dai, Y.; Cao, H.; Qi, C.; Zhao, Y.; Wen, Y.; Xu, C.; Zhong, Q.; Sun, D.; Zhou, S.; Yang, B.; et al. L-cysteine boosted Fe(III)-activated peracetic acid system for sulfamethoxazole degradation: Role of l-cysteine and mechanism. *Chem. Eng. J.* **2023**, *451*, 138588. [[CrossRef](#)]
16. Peng, J.; Wang, Z.; Wang, S.; Liu, J.; Zhang, Y.; Wang, B.; Gong, Z.; Wang, M.; Dong, H.; Shi, J.; et al. Enhanced removal of methylparaben mediated by cobalt/carbon nanotubes (Co/CNTs) activated peroxymonosulfate in chloride-containing water: Reaction kinetics, mechanisms and pathways. *Chem. Eng. J.* **2021**, *409*, 128176. [[CrossRef](#)]
17. Qi, C.; Wen, Y.; Zhao, Y.; Dai, Y.; Li, Y.; Xu, C.; Yang, S.; He, H. Enhanced degradation of organic contaminants by Fe(III)/peroxymonosulfate process with l-cysteine. *Chin. Chem. Lett.* **2022**, *33*, 2125–2128. [[CrossRef](#)]
18. Dai, Y.; Qi, C.; Cao, H.; Wen, Y.; Zhao, Y.; Xu, C.; Yang, S.; He, H. Enhanced degradation of sulfamethoxazole by microwave-activated peracetic acid under alkaline condition: Influencing factors and mechanism. *Sep. Purif. Technol.* **2022**, *288*, 120716. [[CrossRef](#)]
19. Sultana, S.; Hayat, A.; Sayed, M.; Rehan, I.; Rehan, K.; Tabassum, S.; Amin, N.U.; Khan, S.; Khan, A.; Shah, L.A. Photo-Fenton oxidation of dichlorophene in aqueous solution: Kinetics investigation and effects of operational parameters. *Desalin. Water Treat.* **2021**, *222*, 295–301. [[CrossRef](#)]
20. Khan, S.; He, X.; Khan, H.M.; Boccelli, D.; Dionysiou, D.D. Efficient degradation of lindane in aqueous solution by iron(II) and/or UV activated peroxymonosulfate. *J. Photochem. Photobiol. A Chem.* **2016**, *316*, 37–43. [[CrossRef](#)]
21. Khan, S.; Sayed, M.; Sohail, M.; Shah, L.A.; Raja, M.A. Advanced oxidation and reduction processes. *Adv. Water Purif. Tech.* **2019**, 135–164. [[CrossRef](#)]
22. Park, Y.; Kim, S.; Kim, J.; Khan, S.; Han, C. UV/TiO<sub>2</sub> Photocatalysis as an efficient livestock wastewater quaternary treatment for antibiotics removal. *Water* **2022**, *14*, 958. [[CrossRef](#)]
23. Ara, A.; Khattak, R.; Khan, M.S.; Begum, B.; Khan, S.; Han, C. Synthesis, Characterization, and Solar Photo-Activation of Chitosan-Modified Nickel Magnetite Bio-Composite for Degradation of Recalcitrant Organic Pollutants in Water. *Catalysts* **2022**, *12*, 983. [[CrossRef](#)]
24. Khan, S.; Sohail, M.; Han, C.; Khan, J.A.; Khan, H.M.; Dionysiou, D.D. Degradation of highly chlorinated pesticide, lindane, in water using UV/persulfate: Kinetics and mechanism, toxicity evaluation, and synergism by H<sub>2</sub>O<sub>2</sub>. *J. Hazard. Mater.* **2021**, *402*, 123558. [[CrossRef](#)] [[PubMed](#)]
25. Khan, S.; He, X.; Khan, J.A.; Khan, H.M.; Boccelli, D.L.; Dionysiou, D.D. Kinetics and mechanism of sulfate radical-and hydroxyl radical-induced degradation of highly chlorinated pesticide lindane in UV/peroxymonosulfate system. *Chem. Eng. J.* **2017**, *318*, 135–142. [[CrossRef](#)]
26. Nabi, G.; Ain, Q.-U.; Tahir, M.B.; Riaz, K.N.; Iqbal, T.; Rafique, M.; Hussain, S.; Raza, W.; Aslam, I.; Rizwan, M. Green synthesis of TiO<sub>2</sub> nanoparticles using lemon peel extract: Their optical and photocatalytic properties. *Int. J. Environ. Anal. Chem.* **2022**, *102*, 434–442. [[CrossRef](#)]
27. Huang, L.; Weng, X.; Chen, Z.; Megharaj, M.; Naidu, R. Green synthesis of iron nanoparticles by various tea extracts: Comparative study of the reactivity. *Spectrochim. Acta Part A Mol. Biomol. Spectrosc.* **2014**, *130*, 295–301. [[CrossRef](#)]
28. Lu, J.; Batjikh, I.; Hurh, J.; Han, Y.; Ali, H.; Mathiyalagan, R.; Ling, C.; Ahn, J.C.; Yang, D.C. Photocatalytic degradation of methylene blue using biosynthesized zinc oxide nanoparticles from bark extract of *Kalopanax septemlobus*. *Optik* **2019**, *182*, 980–985. [[CrossRef](#)]
29. Veisi, H.; Ghorbani, M.; Hemmati, S. Sonochemical in situ immobilization of Pd nanoparticles on green tea extract coated Fe<sub>3</sub>O<sub>4</sub> nanoparticles: An efficient and magnetically recyclable nanocatalyst for synthesis of biphenyl compounds under ultrasound irradiations. *Mater. Sci. Eng. C.* **2019**, *98*, 584–593. [[CrossRef](#)]
30. Singh, R.K.; Behera, S.S.; Singh, K.R.; Mishra, S.; Panigrahi, B.; Sahoo, T.R.; Parhi, P.K.; Mandal, D. Biosynthesized gold nanoparticles as photocatalysts for selective degradation of cationic dye and their antimicrobial activity. *J. Photochem. Photobiol. A.* **2020**, *400*, 112704. [[CrossRef](#)]

31. Yasin, S.A.; Abbas, J.A.; Saeed, I.A.; Ahmed, I.H. The application of green synthesis of metal oxide nanoparticles embedded in polyethylene terephthalate nanofibers in the study of the photocatalytic degradation of methylene blue. *Polym. Bull.* **2020**, *77*, 3473–3484. [[CrossRef](#)]
32. Rambabu, K.; Bharath, G.; Banat, F.; Show, P.L. Green synthesis of zinc oxide nanoparticles using Phoenix dactylifera waste as bioreductant for effective dye degradation and antibacterial performance in wastewater treatment. *J. Hazard. Mater.* **2021**, *402*, 123560. [[CrossRef](#)]
33. Ali, T.; Warsi, M.F.; Zulfiqar, S.; Sami, A.; Ullah, S.; Rasheed, A.; Alsafari, I.A.; Agboola, P.O.; Shakir, I.; Baig, M.M. Green nickel/nickel oxide nanoparticles for prospective antibacterial and environmental remediation applications. *Ceram. Int.* **2022**, *48*, 8331–8340. [[CrossRef](#)]
34. Danish, M.S.S.; Estrella-Pajulas, L.L.; Alemaida, I.M.; Maria, L.G.; Mikhaylov, A.; Senjyu, T. Green synthesis of silver oxide nanoparticles for photocatalytic environmental remediation and biomedical applications. *Metals* **2022**, *12*, 769. [[CrossRef](#)]
35. Dharmaraj, D.; Krishnamoorthy, M.; Rajendran, K.; Karuppiah, K.; Annamalai, J.; Durairaj, K.R.; Santhiyagu, P.; Ethiraj, K. Antibacterial and cytotoxicity activities of biosynthesized silver oxide (Ag<sub>2</sub>O) nanoparticles using Bacillus paramycoides. *J. Drug Deliv. Sci. Technol.* **2021**, *61*, 102111. [[CrossRef](#)]
36. Aisida, S.O.; Ugwu, K.; Nwanya, A.C.; Bashir, A.; Nwankwo, N.U.; Ahmed, I.; Ezema, F.I. Biosynthesis of silver oxide nanoparticles using leave extract of Telfairia Occidentalis and its antibacterial activity. *Mater. Today Proc.* **2021**, *36*, 208–213. [[CrossRef](#)]
37. Banerjee, K.; Das, S.; Choudhury, P.; Ghosh, S.; Baral, R.; Choudhuri, S.K. A novel approach of synthesizing and evaluating the anticancer potential of silver oxide nanoparticles in vitro. *Chemotherapy* **2017**, *62*, 279–289. [[CrossRef](#)]
38. Laouini, S.E.; Bouafia, A.; Soldatov, A.V.; Algarni, H.; Tedjani, M.L.; Ali, G.A.; Barhoum, A. Green synthesized of Ag/Ag<sub>2</sub>O nanoparticles using aqueous leaves extracts of Phoenix dactylifera L. and their azo dye photodegradation. *Membranes* **2021**, *11*, 468. [[CrossRef](#)]
39. Singh, T.; Jayaprakash, A.; Alsuwaidi, M.; Madhavan, A.A. Green synthesized gold nanoparticles with enhanced photocatalytic activity. *Mater. Today Proc.* **2021**, *42*, 1166–1169. [[CrossRef](#)]
40. Dan, A.; Sengupta, P.K. Synthesis and characterization of polyaniline prepared in formic acid medium. *J. Appl. Polym. Sci.* **2004**, *91*, 991. [[CrossRef](#)]
41. Shah, A.; Haq, S.; Rehman, W.; Waseem, M.; Shoukat, S.; Rehman, M.-U. Photocatalytic and antibacterial activities of paeonia emodi mediated silver oxide nanoparticles. *Mater. Res. Express.* **2019**, *6*, 045045. [[CrossRef](#)]
42. Ravichandran, S.; Paluri, V.; Kumar, G.; Loganathan, K.; Kokati Venkata, B.R. A novel approach for the biosynthesis of silver oxide nanoparticles using aqueous leaf extract of callistemon lanceolatus (myrtaceae) and their therapeutic potential. *J. Exp. Nanosci.* **2016**, *11*, 445–458. [[CrossRef](#)]
43. Shume, W.M.; Murthy, H.; Zereffa, E.A. A review on synthesis and characterization of Ag<sub>2</sub>O nanoparticles for photocatalytic applications. *J. Chem.* **2020**, *2020*, 1–15. [[CrossRef](#)]
44. Wang, X.; Li, S.; Yu, H.; Yu, J.; Liu, S. Ag<sub>2</sub>O as a new visible-light photocatalyst: Self-stability and high photocatalytic activity. *Chem.–A Eur J.* **2011**, *17*, 7777–7780. [[CrossRef](#)] [[PubMed](#)]
45. Saleh, R.; Taufik, A.; Prakoso, S.P. Fabrication of Ag<sub>2</sub>O/TiO<sub>2</sub> composites on nanographene platelets for the removal of organic pollutants: Influence of oxidants and inorganic anions. *Appl. Surf. Sci.* **2019**, *480*, 697–708. [[CrossRef](#)]
46. Khattak, R.; Khan, M.S.; Iqbal, Z.; Ullah, R.; Khan, A.; Summer, S.; Noreen, H.; Zahoor, M.; El-Bahy, S.M.; Batiha, G.E.-S. Catalytic effect of 1,4-dioxane on the kinetics of the oxidation of iodide by dicyanobis(bipyridine)iron(III) in water. *Catalysts* **2021**, *11*, 840. [[CrossRef](#)]
47. Saikia, L.; Bhuyan, D.; Saikia, M.; Malakar, B.; Dutta, D.K.; Sengupta, P. Photocatalytic performance of ZnO nanomaterials for self sensitized degradation of malachite green dye under solar light. *Appl. Catal. A-Gen.* **2015**, *490*, 42–49. [[CrossRef](#)]

**Disclaimer/Publisher’s Note:** The statements, opinions and data contained in all publications are solely those of the individual author(s) and contributor(s) and not of MDPI and/or the editor(s). MDPI and/or the editor(s) disclaim responsibility for any injury to people or property resulting from any ideas, methods, instructions or products referred to in the content.